Physica D 405 (2020) 132396

Contents lists available at ScienceDirect

Physica D

journal homepage: www.elsevier.com/locate/physd

# Effects of precipitation intermittency on vegetation patterns in semi-arid landscapes

L. Eigentler *, J.A. Sherratt

*Maxwell Institute for Mathematical Sciences, Department of Mathematics, Heriot-Watt University, Edinburgh EH14 4AS, United Kingdom*

ARTICLE INFO

*Article history:*
Received 21 August 2019
Received in revised form 4 December 2019
Accepted 5 February 2020
Available online 13 February 2020
Communicated by J. Dawes

*Keywords:*
Impulsive model
Nonlocal dispersal
Pattern formation
Semi-arid landscapes
Precipitation intermittency

ABSTRACT

Patterns of vegetation are a characteristic feature of many semi-arid regions. The limiting resource in these ecosystems is water, which is added to the system through short and intense rainfall events that cause a pulse of biological processes such as plant growth and seed dispersal. We propose an impulsive model based on the Klausmeier reaction–advection–diffusion system, analytically investigate the effects of rainfall intermittency on the onset of patterns, and augment our results by numerical simulations of model extensions. Our investigation focuses on the parameter region in which a transition between uniform and patterned vegetation occurs. Results show that decay-type processes associated with a low frequency of precipitation pulses inhibit the onset of patterns and that under intermittent rainfall regimes, a spatially uniform solution is sustained at lower total precipitation volumes than under continuous rainfall, if plant species are unable to efficiently use low soil moisture levels. Unlike in the classical setting of a reaction–diffusion model, patterns are not caused by a diffusion-driven instability but by a combination of sufficiently long periods of droughts between precipitation pulses and water diffusion. Our results further indicate that the introduction of pulse-type seed dispersal weakens the effects of changes to width and shape of the plant dispersal kernel on the onset of patterns.



## 1. Introduction

Self-organised vegetation patterns are a characteristic feature of semi-arid regions around the world. The formation of patterns is caused by a positive feedback between plant growth and water redistribution towards areas of high biomass [1]. Mechanisms involved in the establishment of such a feedback loop include the formation of infiltration-inhibiting soil crusts in areas of bare ground that induce overland water flow, a combination of strong local water uptake (vertically extended root systems) and fast soil water diffusion, nonlocal water uptake (laterally extended root systems), or a combination thereof [2]. Redistribution of water towards dense biomass patches drives further plant growth in these regions and thus closes the feedback loop. First discovered through areal photography in the 1950s [3], vegetation patterns have been detected in various semi-arid regions of the world (see [4,5] for reviews) such as in the African Sahel [6,7], Somalia [8,9], Australia [10,11], Israel [12,13], Mexico and the US [7,14,15] and northern Chile [16]. The understanding of the evolution and underlying dynamics of patterned vegetation is of crucial importance as changes to properties such as pattern wavelength, recovery time from perturbations or the area fraction colonised by plants may provide an early indication of an irreversible transition to full desert [17–24].

The amount of empirical data on vegetation patterns is limited due to the inability to reproduce patterns in a laboratory setting and the long time scale involved in the formation and evolution of them. Thus, a range of different mathematical models describing the phenomenon have been proposed (in particular by Rietkerk et al. [25] and Gilad et al. [26]), which focus on various different processes that are involved in the formation of vegetation patterns. One model that stands out due to its deliberately basic description of the plant–water-dynamics in semi-arid environments is the Klausmeier model [27]. The excellent framework for mathematical analysis and model extensions provided by the Klausmeier reaction–advection–diffusion model has been utilised extensively in the past (e.g. [28–47]).

Rainfall in semi-arid regions occurs intermittently, seasonally or as a combination of both. Under intermittent rainfall regimes only a small number of short-lasting precipitation events per year provide a sufficiently large amount of water to affect vegetation growing in these regions [48]. If such rainfall events are sufficiently separated, they cause a pulse of biological processes before decay-type phenomena of dry spells take over [48]. Besides plant growth, seed dispersal is also commonly observed to be synchronised with precipitation events. One mechanism,

* Corresponding author.
*E-mail addresses:* le8@hw.ac.uk (L. Eigentler), J.A.Sherratt@hw.ac.uk (J.A. Sherratt).

https://doi.org/10.1016/j.physd.2020.132396
0167-2789/

widespread in dryland ecosystems, which causes such a behaviour is ombrohydrochory, the opening of a seed container due to contact with water [49,50]. Plants in semi-arid regions are sensitive to quantity, frequency and temporal spread of intermittent precipitation events [51–54].

Experimental studies suggest that if the total precipitation volume is kept constant, then a lower frequency of rainfall events yields higher plant biomass [55], an increase in the aboveground net primary productivity [54] and an increase in the seedlings' survival rate [56]. The main factor for these beneficial effects is the temporal increase in soil moisture caused by larger rain events, while a higher number of smaller individual events keeps the moisture level below a threshold needed for the activation of biological processes in plants [54,56]. Contradictory evidence regarding seedling survival exists, which suggests that the effects of rain intermittency depend on a range of factors [55]. In the future, changes to the temporal variability of precipitation (in particular the intensity of rainfall events) are expected to occur globally [57,58].

Despite the fact that seasonality, intermittency and intensity of precipitation have an important influence on semi-desert ecosystems, most mathematical models assume that rainfall occurs continuously and uniformly in time. Some simulation-based studies, however, have addressed the phenomenon by introducing seasonality (i.e. a wet and a dry season) and intermittency of rainfall to existing models for dryland vegetation dynamics. These include modifications of the Rietkerk model [59,60], of the Klausmeier model [37] as well as of the Gilad model [61]. Baudena et al. [62,63] couple a model describing the soil moisture proposed by Laio [64] for the upper soil layer, in which water is added during a wet season either at a constant rate or as an instantaneous event, to vegetation dynamics. The results of these studies show beneficial effects of rainfall intermittency, such as an increase in the area covered by vegetation [61] or plant biomass [61,62] but also suggest that a lower frequency of rain pulses increases the minimum requirement on the total annual precipitation needed to avoid convergence to a bare soil state [37]. The latter result also suggests that the size of the parameter region in which pattern onset occurs reduces under intermittent rainfall regimes [37]. Seasonality of precipitation may have similar effects [59], but can also be detrimental to plants by reducing their biomass and area fraction covered [61,62].

Effects due to changes in the frequency of rainfall events have received very little attention in the mathematical modelling of vegetation patterns, with the works of Ursino and Contarini [37] on the Klausmeier model, Kletter et al. [61] on the Gilad model, and Siteur et al. [60] on the Rietkerk model being notable exceptions. However, none of these papers consider both a wide range of biologically relevant interpulse times and the system dynamics in drought periods. For example, both Kletter et al. and Ursino and Contarini restrict their investigation to a small number of different precipitation frequencies, while Siteur et al. neglect the ecohydrological dynamics between rainfall events. Moreover, most theoretical approaches to study temporal non-uniformity in precipitation are simulation-based. In this paper, we introduce a model based on the Klausmeier model that captures both the impulsive nature of precipitation pulses and associated processes, and also the drought period dynamics. We keep our model sufficiently simple to allow for an analytical investigation of pattern onset in the system. This enables us to consider a wide range of different rainfall regimes and study the effects of precipitation intermittency on the ecohydrological dynamics.

One approach to modelling a system in which pulse-type phenomena occur is the use of integrodifference equations. In separate work [46], we show that such a framework is insufficient to capture effects of precipitation intermittency as it is unable to account for the dynamics specific to drought periods between rainfall pulses. To instead describe situations in which pulse-type phenomena occur alongside the continuous processes of dry spells, impulsive-type systems are used. Such models consist of a system of PDEs describing continuous processes on a finite time domain $(n-1)T < t < nT$, $n \in \mathbb{N}$ and a set of discrete equations that update the densities at times $nT$. The use of impulsive models is a relatively new approach in mathematical modelling but such models are suitable for the description of a wide range of systems. Previous applications include descriptions of populations whose life cycle consists of two non-overlapping stages, such as organisms whose larvae are subjected to a water flow [65,66]; predator prey systems in which consumer reproduction occurs only once a year and is based on the amount of stored energy accumulated through consumption of prey during the year [67] or that are periodically subjected to external inputs [68]; and more general consumer–resource systems in which the consumer reproduction is synchronised [69,70] or in which seasonal harvesting occurs [70]. Impulsive models can further provide a mechanistic interpretation of the underlying ecological processes involved in purely discrete systems [71].

The modelling of plant dispersal as an instantaneous event requires its description by a convolution integral instead of the widely used and mathematically more accessible diffusion term. Biologically, however, this provides a more realistic description of the spatial redistribution of plants as the dynamics of seed dispersal are often affected by nonlocal processes [72]. The use of a convolution term in the description of seed dispersal is thus not a novelty of this paper but has been also been used in a number of previous models for dryland ecosystems [38,73–75].

In this paper, we introduce and analytically study an impulsive model based on the Klausmeier model to gain a better understanding of the effects of pulse-type processes on the onset of vegetation patterns. We motivate the presentation of the model in Section 2 by a review of the Klausmeier model and its most relevant results. In Section 3 we derive conditions for the onset of patterns in the impulsive model based on a linear stability analysis. This allows us to investigate how changes in the rainfall regime affect pattern onset and provides an insight into the mechanism that is responsible for the formation of patterns in the model. The analysis presented in Section 3 is tractable due to some simplifications, such as the use of a specific plant dispersal kernel and the restriction to a flat domain. In Section 4 we augment our analytical results by numerical simulations of extensions of the basic model studied in Section 3 to analyse and discuss the effects of our simplifying assumptions. We present an interpretation of our results and address potential shortfalls in Section 5.

## 2. Model description

In this section we introduce the model which we use to investigate the effects of rainfall intermittency on the onset of patterns in semi-arid environments. We base our model on an extension of the Klausmeier model, whose most relevant results are reviewed.

### 2.1. Klausmeier models

One of the earliest models describing the plant–water dynamics in semi-arid environments is due to Klausmeier [27]. The relative simplicity of the model provides a framework for a rich mathematical analysis (e.g. [29–37]). After a suitable nondimensionalisation [27,29] the model is

$$\frac{\partial u}{\partial t} = \overbrace{u^2 w}^{\text{plant growth}} - \overbrace{Bu}^{\text{plant mortality}} + \overbrace{\frac{\partial^2 u}{\partial x^2}}^{\text{plant dispersal}}, \tag{2.1a}$$

$$\frac{\partial w}{\partial t} = \underbrace{A}_{\text{rainfall}} - \underbrace{w}_{\text{evaporation}} - \underbrace{u^2 w}_{\substack{\text{water consumption}\\ \text{by plants}}} + \underbrace{\nu \frac{\partial w}{\partial x}}_{\substack{\text{water flow}\\ \text{downhill}}} + \underbrace{d \frac{\partial^2 w}{\partial x^2}}_{\text{water diffusion}}, \tag{2.1b}$$

where $u(x,t)$ denotes the plant density, $w(x,t)$ the water density, $x \in \mathbb{R}$ the space domain where $x$ is increasing in the uphill direction and $t > 0$ denotes the time. The diffusion of water was not originally included in the model but is a well established addition [36,76–78]. It is assumed that water is added to the system at a constant rate, evaporation effects are proportional to the water density [79,80] and the plant mortality rate is density-independent. The nonlinearity in the water consumption and plant growth terms arises due to the positive feedback between local vegetation growth and water redistribution. Water uptake by plants is the product of the consumer density ($u$), the resource density ($w$) and a term that accounts for the increased resource availability due to the positive feedback caused, for example, by an increase of soil permeability in vegetated areas ($u$). This nonlinearity drives the formation of spatial patterns. The parameters $A$, $B$, $\nu$ and $d$ represent rainfall, plant loss, the slope and water diffusion, respectively.

The Klausmeier model (2.1) combines all hydrological dynamics into one single variable $w$. By contrast, some other modelling frameworks distinguish between surface water and soil moisture dynamics [25,26]. In this paper, we focus on the modelling framework presented by the Klausmeier model without such a distinction, but the application of our modelling approach to a system with both surface and soil water density is briefly discussed in Section 5.

In a previous paper [38], we have studied the effects of replacing the plant diffusion term in the Klausmeier model by a convolution of a probability density $\phi$ and the plant density $u$, i.e.

$$\frac{\partial u}{\partial t} = u^2 w - Bu + C\left(\phi(\cdot;a) * u(\cdot,t) - u(x,t)\right), \tag{2.2a}$$

$$\frac{\partial w}{\partial t} = A - w - u^2 w + \nu \frac{\partial w}{\partial x} + d \frac{\partial^2 w}{\partial x^2}. \tag{2.2b}$$

The additional parameters $C$ and $a$ represent the rate of plant dispersal and reciprocal width of the dispersal kernel, respectively.

A linear stability analysis of both the local model (2.1) and the nonlocal model (2.2), with the Laplace kernel

$$\phi(x) = \frac{a}{2} e^{-a|x|}, \quad a > 0, x \in \mathbb{R}, \tag{2.3}$$

used in the latter, gives an insight into the nature of patterned solutions of the system. On flat ground, i.e. $\nu = 0$, the onset of spatial patterns occurs due to a diffusion-driven instability. Thus for any level of rainfall $A$, there exists a threshold $d_c \in \mathbb{R}$ on the diffusion coefficient such that an instability occurs for all $d > d_c$. The analysis for the nonlocal model with the Laplace kernel shows that an increase in the width of the dispersal kernel inhibits the formation of patterns by causing an increase in the diffusion threshold.

Unlike the Laplace kernel, other kernel functions do not provide a simplification sufficient to study the onset of patterns analytically. Numerical simulations, however, confirm that the trends observed from the linear stability analysis for the Laplace kernel also apply to other kernel functions [38].

### 2.2. Impulsive model

The Klausmeier model assumes that all processes occur continuously in time. To account for the more realistic combination of pulse-type events associated with short, high intensity precipitation events with the continuous nature of plant loss, water evaporation and water dispersal, we propose an impulsive model to describe the plant and water dynamics in semi-arid environments. Under the assumption that water transport and the decay-type processes of plant mortality and water evaporation are the only processes occurring in drought periods between rainfall pulses [48], the model is

$$\frac{\partial u_n}{\partial t} = \overbrace{-k_1 u_n}^{\text{plant loss}}, \tag{2.4a}$$

$$\frac{\partial w_n}{\partial t} = \underbrace{-k_2 w_n}_{\text{evaporation}} + \underbrace{k_3 \frac{\partial w_n}{\partial x}}_{\substack{\text{water flow}\\ \text{downhill}}} + \underbrace{k_4 \frac{\partial^2 w_n}{\partial x^2}}_{\text{water diffusion}}, \tag{2.4b}$$

$$u_{n+1}(x,0) = \tilde{f}\left(u_n(x,\tau), w_n(x,\tau)\right), \tag{2.4c}$$

$$w_{n+1}(x,0) = \tilde{g}\left(u_n(x,\tau), w_n(x,\tau)\right), \tag{2.4d}$$

where $u_n = u_n(x,t)$, $w_n = w_n(x,t)$, $x \in \mathbb{R}$, $0 < t < \tau$ and $n \in \mathbb{N}$. The spatial domain is considered to be infinite with $x$ increasing in the uphill direction. Between the $(n-1)$-th and $n$th precipitation pulse, the interpulse PDEs (2.4a) and (2.4b) are considered on the finite time domain $0 < t < \tau$, where $\tau$ is the time (in years) between the occurrence of the pulse events described by the update equations (2.4c) and (2.4d). The interpulse PDEs (2.4a) and (2.4b) describe the continuous loss of plants at rate $k_1$, and evaporation at rate $k_2$. While no plant dispersal is assumed to occur during this phase, water diffuses with diffusion coefficient $k_4$ and flows downhill at velocity $k_3$. The simplistic nature of the PDE system allows for an analytical study of conditions for pattern onset to occur (Section 3.1), but an extension which also includes plant growth during drought periods is considered using numerical simulations in Section 4.

The functions $\tilde{f}(u_n(x,\tau), w_n(x,\tau))$ and $\tilde{g}(u_n(x,\tau), w_n(x,\tau))$ in the update equations (2.4c) and (2.4d) describe the system's dynamics during short rainfall pulses, which are assumed to occur periodically in time. To account for plant growth and the associated consumption of water as well as seed dispersal synchronised with a precipitation event, we choose

$$\tilde{f}\left(u_n(x,\tau), w_n(x,\tau)\right) = \overbrace{u_n(x,\tau)}^{\text{existing plants}} + \overbrace{\phi(\cdot;a) * \left(k_5 \left(\frac{u_n(\cdot,\tau)}{k_6 + u_n(\cdot,\tau)}\right)^2 \left(w_n(\cdot,\tau) + \tau k_7\right)\right)}^{\text{dispersal of newly added biomass}},$$

$$\tilde{g}\left(u_n(x,\tau), w_n(x,\tau)\right) = \underbrace{w_n(x,\tau)}_{\text{existing water}} + \underbrace{\tau k_7}_{\text{rainfall}} - \underbrace{\left(\frac{u_n(x,\tau)}{k_6 + u_n(x,\tau)}\right)^2 \left(w_n(x,\tau) + \tau k_7\right)}_{\text{water uptake}}.$$

In the update equation (2.4d) a constant amount water $\tau k_7$ is added to the existing water density. The parameter $k_7$ denotes the total amount of rainfall that occurs over one year and $\tau$ (in years) is the time between two rainfall events. The water volume added to the system during one precipitation event thus is $\tau k_7$. At the same time, water is converted into biomass.

Similar to the Klausmeier model (2.1), the term describing water consumption by plants consists of the total resource density $(w + \tau k_7)$, a term describing the water uptake by the plants' roots $(u/(k_6 + u))$, and a term accounting for the increased ability of plants to consume water in dense patches $u/(k_6 + u)$. As in the Klausmeier model, the functional responses of the latter two to the plant density are chosen to be identical for mathematical convenience. However, the functional response is different

to that used in the Klausmeier model. In the impulsive model $H_{up}(u) = u/(k_6 + u)$, motivated by the saturating behaviour of water infiltration into the soil based on empirical evidence [81] and previous applications in mathematical models [26,82], while in the Klausmeier model $H_{up}(u) = u$. The pulse-type occurrence of precipitation and water uptake in (2.5) necessitates a saturating behaviour ($H_{up}^2(u) < 1$ for all $u \geq 0$) of the functional response to ensure positivity of (2.5d). The parameter $k_6$ is the half saturation constant of the water infiltration and corresponds to the level of plant biomass at which the water infiltration into the soil is at half of its maximum. This water uptake term directly corresponds to the term in (2.4c), describing plant growth, where $k_5$ quantifies the plant species' water to biomass conversion rate. We have numerically tested the model for other nonlinearities in this term with such a saturating behaviour without observing any qualitative differences in the results on pattern onset.

Finally, dispersal of the newly added biomass is described by the convolution term of that biomass with a probability density function $\phi$. This introduces an additional parameter $a$, describing the width of the dispersal kernel in a reciprocal way. This constitutes a second main difference to the models discussed above. While in the Klausmeier models the whole plant density undergoes diffusion/nonlocal dispersal, in the impulsive model only newly added biomass is dispersed, weakening the role of dispersal in the model.

No water redistribution is assumed to occur in this stage. While overland water flow during intense rainfall events is an area of active research [83–85], some hydrological modelling approaches suggest that if the contrast in water infiltration rates between bare and vegetated soil is small (e.g. in non crust-forming soil types such as sandy soil), then no water run-on occurs at plant patches during precipitation pulses [83]. An overview of all parameters, including estimates, is given in Table 2.1.

The formulation of (2.4) is based on a number of simplifying assumptions (e.g. flat terrain, no plant growth during drought periods, linear functional response to the water density in the water consumption term) to make to model analytically tractable (Section 3.1). In Section 4, we relax these assumptions and analyse their effects using numerical methods.

The model can be nondimensionalised by $u = k_6\tilde{u}$, $w = k_5^{-1}k_6\tilde{w}$, $x = a^{-1}\tilde{x}$, $t = k_2^{-1}\tilde{t}$, $A = k_2^{-1}k_5k_6^{-1}k_7$, $B = k_1k_2^{-1}$, $T = k_2\tau$, $\nu = k_2^{-1}k_3a$ and $d = k_2^{-1}k_4a^2$, to give

$$\frac{\partial u_n}{\partial t} = -Bu_n, \tag{2.5a}$$

$$\frac{\partial w_n}{\partial t} = -w_n + \nu\frac{\partial w_n}{\partial x} + d\frac{\partial^2 w_n}{\partial x^2}, \tag{2.5b}$$

$$u_{n+1}(x,0) = u_n(x,T) + \phi(\cdot;1) * \left(\left(\frac{u_n(\cdot,T)}{1+u_n(\cdot,T)}\right)^2 (w_n(\cdot,T) + TA)\right), \tag{2.5c}$$

$$w_{n+1}(x,0) = (w_n(x,T) + TA)\left(1 - \left(\frac{u_n(x,T)}{1+u_n(x,T)}\right)^2\right), \tag{2.5d}$$

after dropping the tildes for brevity, where $u_n = u_n(x,t)$, $w_n = w_n(x,t)$, $x \in \mathbb{R}$, $0 \leq t <\leq$ and $n \in \mathbb{N}$. While the dimensionless parameters $A$, $B$ and $T$ are combinations of several of the original parameters, they can be interpreted as the total amount of rainfall per year, rate of plant loss and time between separate rain and dispersal events, respectively. The water redistribution parameters $\nu$ and $d$ describe the ratio of the water flow coefficients (advection and diffusion, respectively) to the plant dispersal kernel width $1/a$. Their estimates are also included in Table 2.1.

In this form, $T = 4$ corresponds to rain/dispersal events occurring once per year. Even though we present results for $0 < T < 4$ in this paper, it is important to emphasise that ecologically it is meaningless to consider the limit $T \to 0$. As the interpulse time $T$ becomes small, the interpulse PDEs (2.5a) and (2.5b), and in particular the decay-type processes that are described by those equations, become less significant, while the update equations (2.5c) and (2.5d) remain unaffected by changes in $T$. Moreover, substitution of $T = 0$ into (2.5) reduces the impulsive system to an integrodifference system given by (2.5c) and (2.5d) in which no plant death and water evaporation occur. In this setting, due to the lack of water evaporation in the system, resources would be added to the system without being removed, yielding biomass growth without bound.

## 3. Onset of patterns

A common method to study the onset of patterns is linear stability analysis. Spatial patterns occur if a steady state that is stable to spatially homogeneous perturbations becomes unstable if a spatially heterogeneous perturbation is introduced. In this section we apply such an approach to the impulsive model (2.5) on flat ground for the Laplace kernel. Our analysis shows that while a smaller number of strong precipitation events inhibits their onset by decreasing the size of the parameter region supporting the onset of patterns, it also increases the requirements on the total amount of rainfall for plants to persist in a spatially uniform equilibrium. We further show that the introduction of temporal rainfall intermittency replaces water diffusion as the main cause of spatial patterns.

### 3.1. Linear stability analysis

The use of linear stability analysis to determine conditions for the onset of patterns in a system concentrates on the calculation of growth/decay rates of perturbations to a spatially uniform equilibrium. In PDE systems and integrodifference systems, spatially uniform steady states are constant in both space and time, and can be calculated by setting all derivatives to zero (PDE systems) or imposing $u_{n+1} = u_n$ (integrodifference systems). By contrast, spatially uniform equilibria of impulsive systems are not constant in time. Instead, they are periodic in time with period $T$, the time between the occurrences of pulse-type events, and undergo the same cycle during each interpulse period. Consequently, time derivatives in the interpulse PDEs cannot be neglected in the calculation of spatially uniform equilibria. For the given impulsive model

$$\frac{\partial u_n}{\partial t} = -Bu_n, \tag{3.1a}$$

$$\frac{\partial w_n}{\partial t} = -w_n + \nu\frac{\partial w_n}{\partial x} + d\frac{\partial^2 w_n}{\partial x^2}, \tag{3.1b}$$

$$u_{n+1}(x,0) = \tilde{f}\left(u_n(x,T), w_n(x,T)\right), \tag{3.1c}$$

$$w_{n+1}(x,0) = \tilde{g}\left(u_n(x,T), w_n(x,T)\right), \tag{3.1d}$$

where $u_n = u_n(x,t)$, $w_n = w_n(x,t)$, $x \in \mathbb{R}$, $0 < t < T$ and $n \in \mathbb{N}$, the assumption of spatial uniformity reduces the impulsive system to the difference system

$$u_{n+1}(0) = \tilde{f}\left(u_n(0)e^{-BT}, w_n(0)e^{-T}\right), \tag{3.2a}$$

$$w_{n+1}(0) = \tilde{g}\left(u_n(0)e^{-BT}, w_n(0)e^{-T}\right), \tag{3.2b}$$

after solving (3.1a) and (3.1b), where the densities during any interpulse period are given by $u_n(t) = u_n(0)e^{-Bt}$ and $w_n(t) = w_n(0)e^{-t}$ for $0 \leq t \leq T$. Even though a non-trivial equilibrium $(\overline{u}(t), \overline{w}(t))$ of (3.1) is a periodic function of time, we introduce the notations $\overline{u}^0$ and $\overline{w}^0$ to denote the equilibrium densities at the start of the interpulse period, i.e. $\overline{u}^0 := \overline{u}(0)$ and $\overline{w}^0 := \overline{w}(0)$. This

**Table 2.1**
Overview of parameters in (2.4) and (2.5). This table gives an overview of both the dimensional parameters of model (2.4) and the nondimensional parameters of (2.5), including their units (dimensional parameters) or scalings (nondimensional parameters), and their estimated values as well as an interpretation/description. Note that parameter $k_5$ is dimensionless. However, for ease of interpretation, we distinguish between (kg biomass) and (kg $H_2O$). The wide ranges for the water dispersal rates $\nu$ and $d$ arise from their dependence on the variations in the width $a$ of the plant dispersal kernel.

| **Dimensional parameters of** (2.4) | | | |
|---|---|---|---|
| Parameter | Units | Estimates | Description |
| $k_1$ | year$^{-1}$ | 1.8 [27], 0.18 [27], 1.2 [86] | Rate of plant loss |
| $k_2$ | year$^{-1}$ | 4 [27,36,86], 0.2 [25] | Rate of evaporation |
| $k_3$ | m year$^{-1}$ | 0–365 [27] | Velocity of water flow downhill |
| $k_4$ | m$^2$ year$^{-1}$ | 500 [36], | Water diffusion coefficient |
| $k_5$ | (kg biomass) (kg $H_2O$)$^{-1}$ | 0.01 [25], 0.003 [27], 0.002 [27] | Yield of plant biomass per kg water |
| $k_6$ | (kg biomass) m$^{-2}$ | 0.05 [86] | Half saturation constant of water uptake |
| $k_7$ | (kg $H_2O$) m$^{-2}$ year$^{-1}$ | 250–750 [27], 0–1000 [86] | Total amount of rainfall in one year |
| $\tau$ | year | 0–1 | Interpulse time |
| $a$ | m$^{-1}$ | 0.03–100 [72] | Scale parameter of dispersal kernel, reciprocal of the width |
| **Nondimensional parameters of** (2.5) | | | |
| Parameter | Scaling | Estimates | Description |
| $A$ | $k_2^{-1}k_5k_6^{-1}k_7$ | 0–15 [27,36,86] | Precipitation per year |
| $B$ | $k_1k_2^{-1}$ | 0.45 [27], 0.3 [86] 0.045 [27] | Plant mortality rate |
| $T$ | $k_2\tau$ | 0–4 | Interpulse time |
| $\nu$ | $k_2^{-1}k_3a$ | 0–$10^3$ [27,72] | Slope (water flow downhill) |
| $d$ | $k_2^{-1}k_4a^2$ | 0.1–$10^6$ [36,72] | Water diffusion coefficient |

yields that the general, time-dependent equilibrium densities can be written as $\overline{u}(t) = \overline{u}^0e^{-Bt}$ and $\overline{w} = \overline{w}^0e^{-t}$ for $0 \le t \le T$. For brevity, we use the notation $(\overline{u}^0, \overline{w}^0)$ to refer to the equilibrium in the analysis that follows. Thus, from the reduced difference model (3.2) it follows that the equilibria of (3.1) can be found by solving

$$\overline{u}^0 = \tilde{f}\left(\overline{u}^0e^{-BT}, \overline{w}^0e^{-T}\right),$$
$$\overline{w}^0 = \tilde{g}\left(\overline{u}^0e^{-BT}, \overline{w}^0e^{-T}\right).$$

Application of this procedure to (2.5) gives the spatially uniform equilibria of the impulsive system as

$$\begin{aligned}(\overline{u}_d^0, \overline{w}_d^0) &= \left(0, \frac{ATe^T}{e^T-1}\right), (\overline{u}_\pm^0, \overline{w}_\pm^0)\\ &= \left(\frac{\left(AT-2e^{-T}+2\right)e^{-BT} \pm \sqrt{\eta}+2e^{-T}-2}{2e^{-BT}\left(1-e^{-BT}\right)},\right.\\ &\quad \left.\frac{2\left(\left(AT-2e^{-T}+1\right)e^{-BT} \pm \sqrt{\eta}+2e^{-T}-1\right)\left(1-e^{-BT}\right)}{\left(\left(AT-2e^{-T}+2\right)e^{-BT} \pm \sqrt{\eta}+2e^{-T}-2\right)e^{-BT}}\right),\end{aligned}$$

where

$$\begin{aligned}\eta &= \left(4\left(e^{-T}\right)^2+(-4AT-4)e^{-T}+A^2T^2+4AT\right)\left(e^{-BT}\right)^2\\ &\quad +4\left(e^{-T}-1\right)\left(AT-2e^{-T}\right)e^{-BT}+4\left(e^{-T}\right)^2-4e^{-T}.\end{aligned}$$

The steady states $(\overline{u}_\pm^0, \overline{w}_\pm^0)$ only exist provided that

$$A > A_{\min} := \frac{2\left(1-e^{-T}+\sqrt{1-e^{-T}}\right)\left(1-e^{-BT}\right)}{Te^{-BT}}, \tag{3.3}$$

to ensure positivity of $\eta$. In principle, this structure is very similar to that of the Klausmeier models (2.1) and (2.2). For rainfall levels below $A_{\min}$ only the desert steady state $(\overline{u}_d^0, \overline{w}_d^0)$ exists and plants die out, while for sufficiently large amounts of precipitation two further spatially uniform equilibria with non-zero vegetation density exist. An initial conclusion therefore is the existence of an inhibitory effect of long drought periods. The existence threshold $A_{\min}$ of $(\overline{u}_+^0, \overline{w}_+^0)$ increases with the interpulse time $T$ and thus enlarges the parameter region in which the desert equilibrium $(\overline{u}_d^0, \overline{w}_d^0)$ is the only spatially uniform steady state. Even though $A_{\min}$ does not yield any information on the existence of spatially non-uniform solutions for low precipitation levels, we use this threshold as a proxy for the minimum water requirements of the ecosystem. This crucial property is revisited in our discussion on model extensions in Section 4.

Similar to the Klausmeier models, spatial patterns arise from the steady state $(\overline{u}_+^0, \overline{w}_+^0)$ which is stable to spatially homogeneous perturbations (Proposition 3.1). The stability structure of the steady states of the Klausmeier models is preserved in the impulsive model, i.e. the desert steady state $(\overline{u}_d^0, \overline{w}_d^0)$ and the vegetation steady state $(\overline{u}_+^0, \overline{w}_+^0)$ are stable to spatially homogeneous perturbations, while the other vegetation steady state $(\overline{u}_-^0, \overline{w}_-^0)$ is unstable for all biologically realistic parameter choices.

**Proposition 3.1.** *Let* $A > A_{\min}$,

$$\overline{B_2} = \frac{1}{T}\ln\left(1+\frac{ATe^T\sqrt{e^T-1}\left(\sqrt{e^T}-\sqrt{e^T-1}\right)}{2\left(e^T-1\right)}\right),$$

*and* $J_1(B) := e^{-T(B+1)}(\overline{\alpha}\overline{\delta}-\overline{\gamma}\overline{\beta})-1$, *where*

$$\begin{aligned}\overline{\alpha} &= \tilde{f}_u\left(\overline{u}^0e^{-BT}, \overline{w}^0e^{-T}\right), \quad \overline{\beta} = \tilde{f}_w\left(\overline{u}^0e^{-BT}, \overline{w}^0e^{-T}\right),\\ \overline{\gamma} &= \tilde{g}_u\left(\overline{u}^0e^{-BT}, \overline{w}^0e^{-T}\right), \quad \overline{\delta} = \tilde{g}_w\left(\overline{u}^0e^{-BT}, \overline{w}^0e^{-T}\right).\end{aligned} \tag{3.4}$$

*If* $J_1(B)$ *admits a positive real root* $\overline{B_1}$, *the steady state* $(\overline{u}_+^0, \overline{w}_+^0)$ *is stable to spatially homogeneous perturbations if* $B < \min\{\overline{B_1}, \overline{B_2}\}$ *provided that* $\overline{B_2} \in \mathbb{R}$ *or* $B < \overline{B_1}$ *provided that* $\overline{B_2} \notin \mathbb{R}$. *If no positive real solution of* $J_1(B) = 0$ *exists, then* $(\overline{u}_+^0, \overline{w}_+^0)$ *is stable if* $B < \overline{B_2}$ *provided that* $\overline{B_2} \in \mathbb{R}$.

The proof of Proposition 3.1, as well as all those of all other propositions, is deferred until the end of the section.

From Proposition 3.1 it follows that the steady state $(\overline{u}_+^0, \overline{w}_+^0)$ is stable to spatially homogeneous perturbations close to $B =$

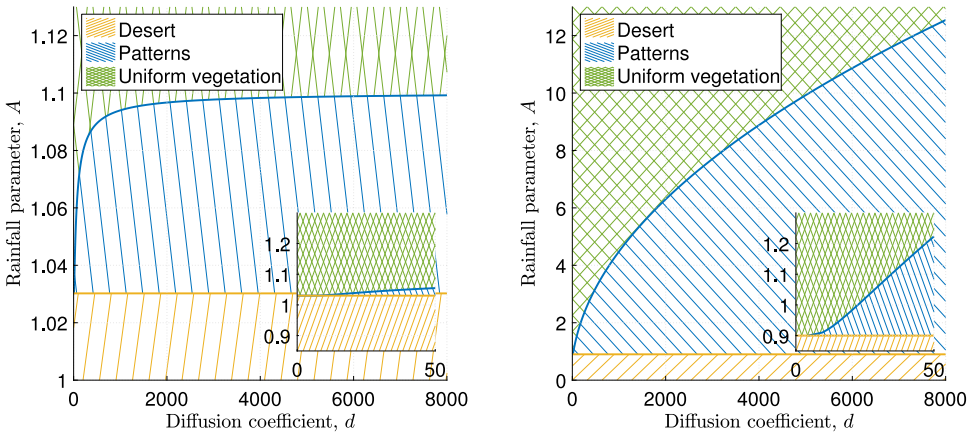


(a) Impulsive model (b) Nonlocal Klausmeier model

**Fig. 3.1.** The stability criterion (3.7) in the $A-d$ parameter plane. Part (a) visualises where the second Jury condition (3.7) changes sign and thus yields an instability, which causes the onset of spatial patterns (blue line). Given some value of $d$, the value of $A$ at which a transition between positivity and negativity of the condition occurs, is determined up to an interval of length $10^{-10}$. The level of $d$ is increased in variable increments. For $d$ close to 0, the increment is chosen to be $\Delta d = 0.1$, which then increases up to $\Delta d = 100$ as the value of $d$ increases. For any given $(A, d)$ pair, (3.7) is evaluated for $k > 0$ at increments of $\Delta k = 0.01$ until a value of $k_c$ is found for which the Jury condition is either negative or positive and increasing. In the former case, the $(A, d)$ pair supports the onset of spatial patterns, in the latter the interval $[k_c - \Delta k, k_c]$ is investigated further with smaller increments in $k$. If still no $k$ is found for which the Jury condition is negative it is assumed that (3.7) is not satisfied. The other parameter values used in this analysis were $T = 0.5$ and $B = 0.45$, with $\phi$ being the Laplacian kernel (2.3). This yields $A_{\min} = 1.03$, and $A_{\max} = 1.099$. A comparison to the nonlocal Klausmeier model, which undergoes a diffusion-driven instability, is shown in (b). Here $A_{\min} = 2B = 0.9$. The insets show the behaviour close to $d = 0$. (For interpretation of the references to colour in this figure legend, the reader is referred to the web version of this article.)

0 for biologically relevant parameters (i.e. $A, T > 0$). Similar calculations yield that $(\overline{u}^0_-, \overline{w}^0_-)$ is unstable close to $B = 0$. In particular, for $B = 0.45$, the highest estimate of the plant mortality parameter (see Table 2.1), the steady state $(\overline{u}^0_+, \overline{w}^0_+)$ is stable for all $(A, T)$ pairs with $A > A_{\min}$, while similarly $(\overline{u}^0_-, \overline{w}^0_-)$ is unstable.

We investigate the existence of spatial patterns by introducing spatially heterogeneous perturbations to the steady state $(\overline{u}^0, \overline{w}^0) := (\overline{u}^0_+, \overline{w}^0_+)$. The following propositions provide conditions for a steady state to be stable to such spatially heterogeneous perturbations and yield results on the effects of rainfall intermittency on the onset of spatial patterns.

**Proposition 3.2.** *Let $\tilde{f}$ be of the form $\tilde{f}(u, w) = u + \phi * \tilde{f}_1(u, w)$. A steady state $(\overline{u}^0, \overline{w}^0)$ of the impulsive model (3.1) is stable to spatially heterogeneous perturbations if $|\lambda(k)| < 1$ for both eigenvalues $\lambda \in \mathbb{C}$ of*

$$J = \begin{pmatrix} \left(1 + \widehat{\phi}(k)\tilde{\alpha}\right) e^{-BT} & \widehat{\phi}(k)\tilde{\beta} e^{-\left(1 - i\nu k + dk^2\right)T} \\ \tilde{\gamma} e^{-BT} & \tilde{\delta} e^{-\left(1 - i\nu k + dk^2\right)T} \end{pmatrix}, \tag{3.5}$$

*for $k > 0$, where*

$$\begin{aligned} \tilde{\alpha} &= \frac{\partial \tilde{f}_1}{\partial u}\left(\overline{u}^0 e^{-BT}, \overline{w}^0 e^{-T}\right), \quad \tilde{\beta} = \frac{\partial \tilde{f}_1}{\partial w}\left(\overline{u}^0 e^{-BT}, \overline{w}^0 e^{-T}\right), \\ \tilde{\gamma} &= \frac{\partial \tilde{g}}{\partial u}\left(\overline{u}^0 e^{-BT}, \overline{w}^0 e^{-T}\right), \quad \tilde{\delta} = \frac{\partial \tilde{g}}{\partial w}\left(\overline{u}^0 e^{-BT}, \overline{w}^0 e^{-T}\right). \end{aligned} \tag{3.6}$$

The entries of the Jacobian (3.5) are complex-valued. However, a significant simplification is achieved by considering the model on flat ground, i.e. the case of $\nu = 0$, thus allowing an application of the Jury criterion (see e.g. [87]) to determine conditions such that $|\lambda(k)| < 1$ for both eigenvalues of the Jacobian.

**Proposition 3.3.** *The steady state $(\overline{u}^0, \overline{w}^0)$ of the impulsive model (3.1) on flat ground is stable to spatially heterogeneous perturbations if*

$$1 + \det(J(k)) - \operatorname{tr}(J(k)) > 0, \tag{3.7}$$

*for all $k > 0$, where $J$ is the Jacobian defined in (3.5) with $\nu = 0$.*

This provides a sufficient condition for the occurrence of spatial patterns. Both the local and the nonlocal Klausmeier models undergo a diffusion-driven instability on flat ground for any level of rainfall, meaning that a sufficiently large ratio of water diffusion rate to plant diffusion rate yields a pattern-inducing instability (see Fig. 3.1(b)). This is not the case for the impulsive model. For sufficiently high levels of rainfall, patterns cannot occur for any level of the diffusion coefficient $d$, the ratio of the water diffusion rate to the plant dispersal kernel width. It is indeed the time $T$ between rainfall pulses that determines for which levels of precipitation patterns can form. Only for smaller values of $A$ an increase of diffusion through the critical value $d_c(A)$ causes an instability and thus the onset of patterns. Reverting back to parameters in dimensional form, this also shows that for sufficiently low precipitation levels, wider plant dispersal kernels inhibit the onset of patterns, which is in agreement with results from the nonlocal Klausmeier model (2.2) [38]. Similar to the Klausmeier models, diffusion levels close to $d = 0$ do not yield an instability for any rainfall parameters and there is a direct transition from the stable plant steady state to the desert steady state as $A$ is decreased through the lower bound $A_{\min}$. This is a conclusion of a numerical investigation (Fig. 3.1) of the stability condition (3.7) using the Laplace kernel (2.3) in the $A - d$ parameter plane. This analysis was performed for various different choices of the parameters $B$ and $T$ without showing any qualitative differences.

The evaluation of (3.7) in the $A - d$ parameter plane suggests a closer investigation of the stability condition (3.7) for $d \to \infty$ (Proposition 3.4) and $A = A_{\min}$ (Proposition 3.6). The former provides information on the level of rainfall $A_{\max}$ above which no instability can occur, while the latter yields the locus of $d_{A_{\min}}$, the minimum value of diffusion required for an instability to occur.

**Proposition 3.4.** *If $d \to \infty$ in the impulsive model (3.1) on flat ground with the Laplace kernel (2.3), then $(\overline{u}^0, \overline{w}^0)$ is unstable to spatially heterogeneous perturbations if $A < A_{\max}$, where $A_{\max}$*

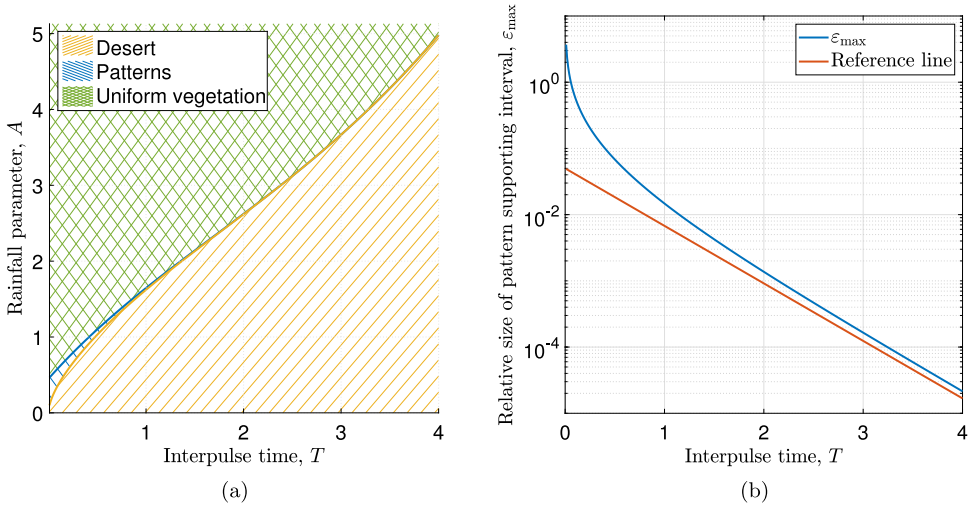


**Fig. 3.2.** Classification of the $A-T$ parameter plane and the relative size of the rainfall interval supporting pattern onset as $d \to \infty$. Part (a) shows a classification of the $A-T$ parameter plane in the limit $d \to \infty$ into regions in which uniform vegetation is stable, in which pattern onset occurs, and in which the desert state is the only spatially uniform equilibrium of the system. The transition $A = A_{max}$ between uniform and patterned vegetation (blue line) is obtained by numerically solving (3.8), while the lower bound $A = A_{min}$ on the parameter region supporting pattern onset (yellow line) is obtained from the analytic condition (3.3). The relative size $\varepsilon_{max} := A_{max} - A_{min}$ of the parameter region supporting pattern onset is visualised in (b) and is compared to a reference line of slope $\exp(-2T)$. The plant loss parameter is $B = 0.45$ Note the logarithmic scale in (b). (For interpretation of the references to colour in this figure legend, the reader is referred to the web version of this article.)

*satisfies*

$$(1 + \tilde{\alpha}(A_{max}))\, e^{-BT} - 1 = 0. \tag{3.8}$$

**Corollary 3.5.** *The relative size* $(A_{max} - A_{min})/A_{min}$ *of the interval* $[A_{min}, A_{max}]$ *is proportional to* $e^{-2T}$ *as* $T \to \infty$.

Given a set of parameters $(B, T)$, (3.8) can be solved numerically to provide the level of rainfall $A$ at which a transition between uniform and patterned vegetation occurs in the limit $d \to \infty$. In combination with the preceding results, this is the threshold $A_{max}$ beyond which no pattern onset can occur. This is in stark contrast to the classical case of a diffusion-driven instability which occurs in the Klausmeier models (2.1) and (2.2) for which $A_{max} \to \infty$ as $d \to \infty$. Together with the lower bound on the rainfall parameter $A_{min}$ this allows a classification of the $T-A$ parameter plane into three regions (Fig. 3.2(a)); one in which the desert steady state is the only spatially uniform equilibrium to exist, one in which instability of the uniform plant steady state to spatially heterogeneous perturbations causes the onset of spatial patterns, and one in which any perturbations of the equilibrium $(\overline{u}^0, \overline{w}^0)$ decay and no pattern onset occurs. This classification of the $T-A$ parameter plane is based on the preceding linear stability analysis and the perturbation of the spatially uniform equilibrium $(\overline{u}^0, \overline{w}^0)$. This results in a classification that provides information regarding the onset of patterns but does not yield any knowledge of the existence of patterns away from their onset. While no systematic study of the whole parameter space using numerical continuation was performed, patterns for parameters outside the interval given by the linear stability analysis can be observed by slowly increasing/decreasing the rainfall parameter $A$ beyond/below the pattern onset-supporting interval when the system is already in a patterned state.

Proposition 3.4 indicates that a decrease in the frequency of precipitation events requires a higher amount of rainfall to avoid an instability. This does not mean that pattern onset occurs for a larger parameter range as periods of droughts become longer, as an increase in $T$ also increases the lower bound on the rainfall for the vegetation steady state to exist. Indeed, Corollary 3.5 provides information on the size of the interval for the rainfall parameter $A$ that supports the onset of patterns relative to the lower bound (3.3) on the rainfall (Fig. 3.2(b)). For small values of $T$ the size of this interval is larger than the lower bound on the rainfall, for larger $T$ the size of the pattern onset-supporting interval of rainfall levels decreases at a rate proportional to $e^{-2T}$.

For $A = A_{min}$, the previous analysis (Fig. 3.1(a)) suggests the existence of a threshold $d_{A_{min}}$ on the diffusion coefficient $d$ below which no instability occurs. Similar to the Klausmeier models (2.1) and (2.2) this corresponds to a direct transition between the spatially uniform vegetation state and the desert state as the rainfall parameter $A$ decreases through $A_{min}$.

**Proposition 3.6.** *If* $A = A_{min}$, *there exists a threshold* $d_{A_{min}} > 0$ *such that* $(\overline{u}^0, \overline{w}^0)$ *is unstable to spatially heterogeneous perturbations for* $d > d_{A_{min}}$.

The threshold given by Proposition 3.6 is independent of the plant loss parameter $B$. Plant mortality does, however, affect $A_{min}$, the level of rainfall required for the plant steady state to exist. The simplification provided by setting $A = A_{min}$ is not sufficient to determine the threshold $d_{A_{min}}$ on the diffusion coefficient explicitly, but similar to the analysis in the $d \to \infty$ case, it can be determined numerically for a given set of parameters. The results of this show that an increase in the time interpulse $T$ causes an increase in the threshold $d_{A_{min}}$ on the diffusion coefficient, i.e. a higher ratio of water diffusion to plant dispersal kernel width is required to cause an instability leading to the onset of patterns.

**Proof of Proposition 3.1.** Linear stability analysis of a steady state $(\overline{u}^0, \overline{w}^0)$ of the impulsive model (3.1) in a spatially uniform setting is equivalent to linear stability analysis of the difference system (3.2) with $\tilde{f}(u, w) = u + (u/(1+u))^2(w + TA)$ and $\tilde{g}(u, w) = (w + TA)(1 - (u/(1+u))^2)$. Linearisation about the steady state and introduction of a perturbation proportional to $\lambda^n$ yield that the growth factor $\lambda \in \mathbb{C}$ is an eigenvalue of the Jacobian

$$J(\overline{u}^0, \overline{w}^0) = \begin{pmatrix} e^{-BT}\overline{\alpha} & e^{-T}\overline{\beta} \\ e^{-BT}\overline{\gamma} & e^{-T}\overline{\delta} \end{pmatrix}.$$

The Jury conditions then yield stability of a steady state $(\overline{u}^0, \overline{w}^0)$ if

$$e^{-T(B+1)}\left(\overline{\alpha}\overline{\delta} - \overline{\gamma}\overline{\beta}\right) < 1, \tag{3.9a}$$

$$1 + e^{-T(B+1)}\left(\overline{\alpha}\overline{\delta} - \overline{\gamma}\overline{\beta}\right) > \left|e^{-BT}\overline{\alpha} + e^{-T}\overline{\delta}\right|, \tag{3.9b}$$

are both satisfied.

The first Jury condition (3.9a) yields $J_1(B) < 0$. For $(\overline{u}^0, \overline{w}^0) = (\overline{u}^0_+, \overline{w}^0_+)$, $J_1(0) = -1$ and thus the condition is satisfied for $B < \overline{B_1}$, where $\overline{B_1}$ is the smallest real positive root of $J_1(B)$ provided it exists. The second Jury condition (3.9b) is $J_2(B) := 1+e^{-T(B+1)}(\overline{\alpha}\overline{\delta}-\overline{\beta}\overline{\gamma})-e^{-BT}\overline{\alpha}-e^{-T}\overline{\delta} > 0$. For $(\overline{u}^0, \overline{w}^0) = (\overline{u}^0_+, \overline{w}^0_+)$, $J_2(0) = 0$ and $\mathrm{d}J_2/\mathrm{d}B(0) = T > 0$ and thus the condition is satisfied for $B < \overline{B_2}$, which is the smallest real positive root of $J_2(B)$ provided it exists. □

**Proof of Proposition 3.2.** Similar to Proposition 3.1, this proof is based on a linear stability analysis. Unlike in the proof of Proposition 3.1, the system cannot be immediately reduced to a difference system. Additionally, the convolution in (3.1c) adds a complication. However, both these issues can be addressed by performing the analysis in Fourier space.

As is standard with linear stability analysis, we investigate the behaviour of perturbations $(\tilde{u}(x,t), \tilde{w}(x,t))$ to a spatially uniform equilibrium $(\overline{u}(t), \overline{w}(t)) = (\overline{u}^0 e^{-Bt}, \overline{w}^0 e^{-t})$ by setting

$$u_n(x,t) = \overline{u}^0 e^{-Bt} + \tilde{u}(x,t) \quad \text{and} \quad w_n(x,t) = \overline{w}^0 e^{-t} + \tilde{w}(x,t). \tag{3.10}$$

Substitution into the update equations (3.1c) and (3.1d) and linearisation yields

$$\tilde{u}_{n+1}(x,0) = \tilde{u}_n(x,T) + \phi * \left(\tilde{\alpha}\tilde{u}_n(\cdot,T) + \tilde{\beta}\tilde{w}_n(\cdot,T)\right), \tag{3.11a}$$

$$\tilde{w}_{n+1}(x,0) = \tilde{\gamma}\tilde{u}_n(x,T) + \tilde{\delta}\tilde{w}_n(x,T), \tag{3.11b}$$

noting that $\tilde{g}(\overline{u}^0 e^{-BT}, \overline{w}^0 e^{-T}) = \overline{w}^0$ and $\tilde{f}_1(\overline{u}^0 e^{-BT}, \overline{w}^0 e^{-T}) = \overline{u}^0(1-e^{-BT})$ by the definition of the spatially uniform equilibria. The Fourier transform applied to (3.11) gives

$$\widehat{\tilde{u}_{n+1}}(k,0) = \left(1 + \widehat{\phi}(k)\tilde{\alpha}\right)\widehat{\tilde{u}_n}(k,T) + \widehat{\phi}(k)\tilde{\beta}\widehat{\tilde{w}_n}(k,T), \tag{3.12a}$$

$$\widehat{\tilde{w}_{n+1}}(k,0) = \tilde{\gamma}\widehat{\tilde{u}_n}(k,T) + \tilde{\delta}\widehat{\tilde{w}_n}(k,T), \tag{3.12b}$$

making use of the convolution theorem. The functions $\widehat{\tilde{u}_n}$ and $\widehat{\tilde{w}_n}$ satisfy the interpulse PDEs (3.1a) and (3.1b). Taking the Fourier transform of the interpulse PDEs (3.1a) and (3.1b) gives

$$\frac{\partial\widehat{\tilde{u}_n}(k,t)}{\partial t} = -B\widehat{\tilde{u}_n}(k,t), \quad \frac{\partial\widehat{\tilde{w}_n}(k,t)}{\partial t} = -(1 - i\nu k + dk^2)\widehat{\tilde{w}_n}(k,t),$$

which can be solved to

$$\widehat{\tilde{u}_n}(k,t) = \widehat{\tilde{u}_n}(k,0)e^{-Bt}, \quad \widehat{\tilde{w}_n}(k,t) = \widehat{\tilde{w}_n}(k,0)e^{-(1-i\nu k+dk^2)t}. \tag{3.13}$$

Substitution into (3.12) yields

$$\widehat{\tilde{u}_{n+1}}(k,0) = \left(1 + \widehat{\phi}(k)\tilde{\alpha}\right)e^{-BT}\widehat{\tilde{u}_n}(k,0) + \widehat{\phi}(k)\tilde{\beta}e^{-(1-i\nu k+dk^2)T}\widehat{\tilde{w}_n}(k,0),$$

$$\widehat{\tilde{w}_{n+1}}(k,0) = \tilde{\gamma}e^{-BT}\widehat{\tilde{u}_n}(k,0) + \tilde{\delta}e^{-(1-i\nu k+dk^2)T}\widehat{\tilde{w}_n}(k,0).$$

from (3.12). This is a linear difference system to which standard tools of stability analysis can be applied. In other words, the assumption that the perturbations $\widehat{\tilde{u}_n}$ and $\widehat{\tilde{w}_n}$ are proportional to $\lambda^n$ yields that the growth factor $\lambda \in \mathbb{C}$ is an eigenvalue of the Jacobian $J$. □

**Proof of Proposition 3.3.** To investigate a steady state's stability on flat ground, the Jury conditions can be used. An instability occurs, if at least one of

$$\det(J) - 1 < 0, \tag{3.14a}$$

$$1 + \det(J) - |\mathrm{tr}(J)| > 0, \tag{3.14b}$$

is not satisfied for some $k > 0$. The first Jury condition (3.14a) is automatically satisfied due to stability to spatially homogeneous perturbations, because

$$\begin{aligned}\det(J) &= e^{-T\left(B+1+dk^2\right)}\left(\left(1+\widehat{\phi}(k)\tilde{\alpha}\right)\tilde{\delta} - \widehat{\phi}(k)\tilde{\beta}\tilde{\gamma}\right)\\ &= e^{-T\left(B+1+dk^2\right)}\left(\tilde{\delta} + \widehat{\phi}(k)\left(\tilde{\alpha}\tilde{\delta} - \tilde{\beta}\tilde{\gamma}\right)\right)\\ &< e^{-T(B+1)}\left(\tilde{\delta} + \tilde{\alpha}\tilde{\delta} - \tilde{\beta}\tilde{\gamma}\right) = e^{-T(B+1)}\left(\overline{\alpha}\overline{\delta} - \overline{\beta}\overline{\gamma}\right) < 1,\end{aligned}$$

for all $k > 0$, noting that $1 + \tilde{\alpha} = \overline{\alpha}$, $\tilde{\beta} = \overline{\beta}$, $\tilde{\gamma} = \overline{\gamma}$ and $\tilde{\delta} = \overline{\delta}$, where $\overline{\alpha}$, $\overline{\beta}$, $\overline{\gamma}$ and $\overline{\delta}$ are defined in (3.4). The last inequality makes use of the steady state's stability to spatially homogeneous perturbations, which in particular guarantees that (3.9a) holds. Therefore, assuming a steady state's stability to spatially homogeneous perturbations, a sufficient condition for spatial patterns to occur is the existence of some wavenumber $k > 0$ such that the second Jury condition (3.7) does not hold. In the case of model (2.5) this condition can be slightly simplified by noting that $\tilde{\alpha} > 0$ and $\tilde{\delta} > 0$ and therefore $\mathrm{tr}(J) > 0$ for all $k > 0$. The condition thus becomes $1 + \det(J) - \mathrm{tr}(J) > 0$. □

**Proof of Proposition 3.4.** If $d \to \infty$ and $\nu = 0$, then the Jacobian (3.5) becomes

$$J = \begin{pmatrix} \left(1+\widehat{\phi}(k)\tilde{\alpha}\right)e^{-BT} & 0 \\ \tilde{\gamma}e^{-BT} & 0 \end{pmatrix}.$$

Its determinant is clearly zero and therefore the stability condition simplifies to $1 - (1 + \widehat{\phi}(k)\tilde{\alpha})e^{-BT} > 0$, for all $k > 0$. For the Laplacian kernel (2.3) this is a polynomial in $k^2$, which after rearranging becomes

$$k^2 > \frac{\left(\left(1+\tilde{\alpha}\right)e^{-BT} - 1\right)}{1 - e^{-BT}}. \tag{3.15}$$

Stability of the steady state requires (3.15) to hold for all $k > 0$. This is only possible if the right hand side of (3.15) is negative. Thus, an instability causing the onset of spatial patterns occurs if

$$\left(1+\tilde{\alpha}\right)e^{-BT} - 1 > 0. \tag{3.16}$$

The coefficient $\tilde{\alpha}$ is decreasing in $A$ and thus there exists a threshold $A = A_{\max}$ such that an instability occurs for all $A < A_{\max}$. □

**Proof of Corollary 3.5.** Substitution of $A = A_{\min}(1+\varepsilon)$ into (3.16) gives

$$\varepsilon < \varepsilon_{\max} := \frac{1}{8\left(e^{\frac{3T}{2}}\sqrt{e^T-1} + e^{2T} - e^{\frac{T}{2}}\sqrt{e^T-1} - e^T\right)},$$

after linearisation in $\varepsilon$. The right hand side $\varepsilon_{\max}$ denotes the relative size of the rainfall interval supporting pattern onset. Its logarithm decreases at rate

$$\begin{aligned}\left(\ln\left(\varepsilon_{\max}\right)\right)' &= -\frac{4e^{\frac{3T}{2}}\sqrt{e^T-1} + 4e^{2T} - 2e^{\frac{T}{2}}\sqrt{e^T-1} - 5e^T + 1}{2\sqrt{e^T-1}\left(e^T\sqrt{e^T-1} + e^{\frac{3T}{2}} - \sqrt{e^T-1} - e^{\frac{T}{2}}\right)}\\ &\to -2 \quad \text{as} \quad T \to \infty.\end{aligned}$$

This shows the exponential decay of the relative interval size $\varepsilon_{\max}$. □

**Proof of Proposition 3.6.** Setting $A = A_{\min}$ provides a significant simplification as the equilibrium becomes

$$\left(\overline{u}^0, \overline{w}^0\right) = \left(\sqrt{1-e^{-T}}e^{BT}, \frac{\left(e^{BT}-1\right)\left(1+2\sqrt{1-e^{-T}}\right)}{\sqrt{1-e^{-T}}}\right).$$

Thus the coefficients $\tilde{\alpha}$, $\tilde{\beta}$, $\tilde{\gamma}$ and $\tilde{\delta}$ given by (3.6) become

$$\tilde{\alpha}_{A_{\min}} = \frac{2\left(e^{BT}-1\right)\left(2-e^{-T}+2\sqrt{1-e^{-T}}\right)}{\left(1+\sqrt{1-e^{-T}}\right)^3},$$

$$\tilde{\beta}_{A_{\min}} = \frac{1-e^{-T}}{\left(1+\sqrt{1-e^{-T}}\right)^2},$$

$$\tilde{\gamma}_{A\min} = -\tilde{\alpha}_{A_{\min}},$$

$$\tilde{\delta}_{A_{\min}} = \frac{2\sqrt{1-e^{-T}}+1}{\left(1+\sqrt{1-e^{-T}}\right)^2},$$

respectively. The Jacobian (3.5) then is

$$J_{A_{\min}} = \begin{pmatrix} \left(1+\widehat{\phi}(k)\tilde{\alpha}_{A_{\min}}\right)e^{-BT} & \widehat{\phi}(k)\tilde{\beta}_{A_{\min}}e^{-\left(1+dk^2\right)T} \\ \tilde{\gamma}_{A_{\min}}e^{-BT} & \tilde{\delta}_{A_{\min}}e^{-\left(1+dk^2\right)T} \end{pmatrix},$$

and hence the steady state $(\overline{u}^0, \overline{w}^0)$ is stable to spatially heterogeneous perturbations if

$$1+\det\left(J_{A_{\min}}\right)-\operatorname{tr}\left(J_{A_{\min}}\right) = \zeta\left(1-e^{-BT}\right) > 0 \Longleftrightarrow \zeta > 0,$$
$$\text{for all} \quad k > 0 \tag{3.17}$$

where

$$\begin{aligned}\zeta = \frac{1}{\left(e^{T/2}+\sqrt{e^T-1}\right)^3}\Big(&\left(\left(-2\tilde{\beta}_{A_{\min}}-2\tilde{\delta}_{A_{\min}}\right)\widehat{\phi}(k)\right.\\ &\left.+\ 3\tilde{\delta}_{A_{\min}}\right)e^{-Tdk^2-T/2}\\ &+\left(\left(4\tilde{\beta}_{A_{\min}}+4\tilde{\delta}_{A_{\min}}\right)\widehat{\phi}(k)-4\tilde{\delta}_{A_{\min}}\right)e^{-Tdk^2+T/2}\\ &+\sqrt{e^T-1}e^{-\left(dk^2+1\right)T}\tilde{\delta}_{A_{\min}}\\ &+4\sqrt{e^T-1}\left(\left(\tilde{\beta}_{A_{\min}}+\tilde{\delta}_{A_{\min}}\right)\widehat{\phi}(k)-\tilde{\delta}_{A_{\min}}\right)e^{-Tdk^2}\\ &+\left(-1+\left(4-4\widehat{\phi}(k)\right)e^T\right)\sqrt{e^T-1}+\left(-3+2\widehat{\phi}(k)\right)e^{T/2}\\ &-4e^{3/2T}\left(\widehat{\phi}(k)-1\right)\Big).\end{aligned}$$

The minimum of the function $\zeta$ is decreasing in $d$ and thus there exists a threshold $d_{A_{\min}}$ such that (3.17) does not hold for any $d > d_{A_{\min}}$. □

## 4. Simulations of model extensions

In the preceding linear stability analysis we have made a number of simplifying assumptions to make the derivation of the criteria for pattern onset analytically tractable. To investigate the impact of these simplifications on our results, we numerically investigate extensions of (2.5) in which some previous assumptions are relaxed.

The analysis in this section yields that the exponential decay (with increasing $T$) of the size of the parameter region supporting pattern onset is due to the temporal separation of the components of the pattern-inducing feedback loop and does not occur if plant growth processes extend into drought periods. Results obtained in this section also highlight the importance of understanding a plant species' response to low soil moisture levels. This functional response is established to have an important influence on the ecosystem dynamics under precipitation regimes with intermediate interpulse times. Finally, the effects of sloped terrain and changes to the plant dispersal kernel are investigated.

### 4.1. Method

Simulations to determine the parameter region in which pattern onset occurs are performed in two stages. Unless the non-trivial spatially uniform equilibria of the system can be calculated analytically, we initially integrate the corresponding space-independent model to determine the threshold $A_{\min}$ below which the desert equilibrium is the system's only spatially uniform steady state. The calculation of $A_{\min}$ further provides the equilibrium plant and water densities $(\overline{u}^0, \overline{w}^0)$ close to the threshold.

Simulations of the full model are then performed on the space domain $[-x_{\max}, x_{\max}]$ centred at $x = 0$. This domain is discretised into $M$ equidistant points $x_1, \dots, x_M$ with $-x_{\max} = x_1 < x_2 < \cdots < x_M = x_{\max}$ such that $\Delta x = x_2 - x_1 = \cdots = x_M - x_{M-1}$. The ODE system resulting from the discretisation of the interpulse PDE system (2.5a) and (2.5b) is integrated, and the densities at every space point are updated at the end of each interpulse period of length $T$. The discrete convolution term arising from the discretisation of (2.5c) is obtained by using the convolution theorem and the fast Fourier transform, providing a significant simplification through a reduction of the number of operations from $O(M^2)$ to $O(M\log(M))$ required to obtain the convolution (see e.g. [88]).

To mimic the infinite domain used for the linear stability analysis (Section 3.1), we define the initial condition of the system as follows; on a subdomain $[-x_{\text{sub}}, x_{\text{sub}}]$ centred at $x = 0$ of the domain $[-x_{\max}, x_{\max}]$ the steady state $(\overline{u}^0, \overline{w}^0)$ near its existence threshold $A_{\min}$ is perturbed by a function containing a collection of applicable spatial modes, while on the rest of the domain the densities are initially set to equal the densities of the steady state $(\overline{u}^0, \overline{w}^0)$. The restriction of the perturbations to a small subdomain is used to avoid difficulties posed by the boundaries. The size of the outer domain is therefore chosen large enough so that any boundary conditions (which are set to be periodic) that are imposed on $[-x_{\max}, x_{\max}]$ do not affect the solution in the subdomain during the time that is considered in the simulation. Fig. 4.1 shows a typical patterned solution obtained by these simulations.

We use model realisations obtained through this method to determine the critical rainfall level $A_{\max}$ below which pattern onset occurs in the different model extensions.

### 4.2. Nonlinear water uptake

In the original model (2.5), water consumption by plants (and the plant growth associated with it) is described by

$$\text{Up}(u,w) = G_{\text{up}}(w)H_{\text{up}}^2(u) = (w+TA)\left(\frac{u}{1+u}\right)^2.$$

The linearity in $w$ is inherited from the Klausmeier model on which our impulsive model is based. Field observations indicate that dryland ecosystems remain dormant under low soil moisture levels and are only activated if the water density is sufficiently high [54,56]. Mathematically, such a property can be described by a Holling type III functional response [89]. To incorporate such a nonlinear response into the impulsive model, we consider an amended uptake function with

$$\widetilde{G_{\text{up}}}(w) = \frac{C_m\,(w+TA)^p}{C_h^p+(w+TA)^p}, \quad p > 1,$$

where $C_m$ is the maximum water uptake per unit biomass, $C_h$ is the half saturation constant of the water consumption and $p$ accounts for the strength of the nonlinearity. Typical parameter values are $C_m = 20$, $C_h = \sqrt{2}$ and $p = 4$ [89]. The introduction of this nonlinearity causes complications as positivity of the water

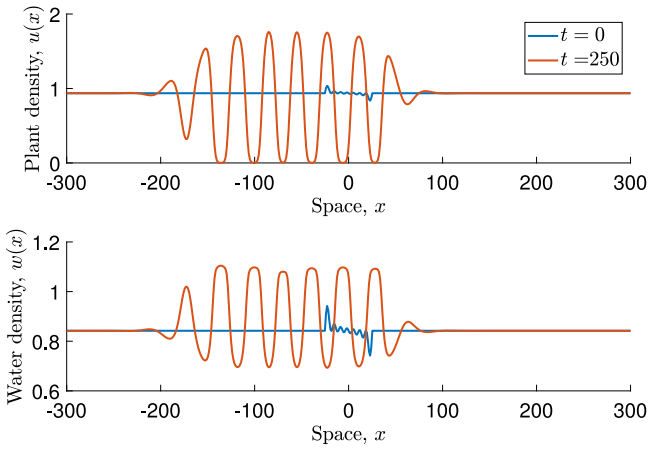


**Fig. 4.1.** Solution of the impulsive model. This visualises a numerically obtained realisation of the impulsive model (2.5) on flat ground. The plant dispersal kernel $\phi$ is set to the Laplacian kernel (2.3) and the parameter values are $B = 0.45$, $A = 1.623$, $d = 100$ and $T = 1$. The number of space points is $M = 10^9$.

density $w$ is no longer guaranteed by the update equation (2.5d). To avoid the occurrence of negative densities, we cap the new water uptake function $\widetilde{\text{Up}}(u, w)$ by $w + TA$, i.e. set

$$\widetilde{\text{Up}}(u, w) = \max\{w + TA, \widetilde{G_{\text{up}}}(w)\}H_{\text{up}}^2(u).$$

The most significant result of our numerical investigation of (2.5) with a Holling type III functional response in the water uptake and plant growth terms is that the minimum of the existence threshold $A_{\min}$ of a non-trivial equilibrium (Fig. 4.2(a)) occurs for intermediate interpulse times. Under the assumption that total annual rainfall $A$ is fixed, longer drought periods between precipitation pulses correspond to higher intensity rainfall events. Resource availability at the time of water uptake and plant growth is thus higher and exceeds the threshold required for plant growth processes to be activated, which is accounted for in the Holling type III functional response. Conversely, high frequency–low intensity precipitation pulses accumulating to the same amount of total annual rainfall volume are not sufficient to push the water density above this critical value. It is worth emphasising that further increases in the separation of precipitation events (and associated increases in rainfall intensity) to a low frequency–high intensity regime reverses the decrease in $A_{\min}$ due to the saturating behaviour of the water uptake function.

Further, the property that an increase in the interpulse time $T$ reduces the size of the parameter region in which onset of patterns occurs is unaffected by the introduction of a nonlinear water uptake term. Similar to the analytically derived exponential decay of the relative size of $[A_{\min}, A_{\max}]$ for (2.5) with a linear functional response (Corollary 3.5), results of our numerical scheme for a Holling type III functional response also indicate an exponential decay of the interval's relative size with increasing interpulse times (Fig. 4.2(b)).

Numerical solutions of the model do, however, become unreliable as the interpulse time $T$ is increased. For larger $T$, the decay-type processes in the interpulse PDEs yield very low plant levels in the troughs of the pattern at the end of the interpulse period. This is a natural source of potential errors. Indeed, Fig. 4.2(c) depicts that numerical solutions of the system for large $T$ can yield negative plant densities at the end of the interpulse period, highlighting the difficulties encountered in a numerical approach.

To investigate the effects of the strength of the nonlinearity in more detail, we compare results on pattern onset as the strength of the nonlinearity gradually increases away from the linear behaviour considered in (2.5). While it is impossible to revert back to the linear term by parameter changes only, the behaviour for small values of the water density $w$ can be mimicked by choosing $p = 1$ and $C_m = C_h$ sufficiently large. We use this as the reference point to the analytical results obtained in Section 3.1 and vary the extent of the nonlinearity in the functional response by fixing $C_m = 20$ and setting $C_h = 20 - (20 - \sqrt{2})\xi$ and $p = 1 + 3\xi$ for $0 \le \xi \le 1$. For sufficiently low fixed interpulse times $T$, an initial increase of $\xi$ causes an increase of the rainfall level $A_{\min}$ that is required for a spatially uniform non-trivial equilibrium to exist (Fig. 4.2(d)). As the strength of the nonlinearity increases further, $A_{\min}$ attains a maximum and then decreases below its level for the model with linear functional water uptake response analysed in Section 3.1.

The reasoning for this behaviour stems from the variation in the functional response $G_{\text{up}}$ under changes of $\xi$, which is visualised in Fig. 4.2(e). For sufficiently low $T$, the resource availability at the time of water uptake is also low. Thus a linear functional response yields a higher water consumption than a nonlinear response with moderate $\xi$, but a lower consumption than a nonlinear response with larger $\xi$. More precisely, the increase in the exponent $p$ and the associated concave-up shape of $G_{\text{up}}$ causes the initial increase in $A_{\min}$. A further increase in $\xi$ decreases the half-saturation parameter $C_h$ and the range of resource densities affected by the concave-up behaviour decreases in size. This causes the eventual decrease in $A_{\min}$ as the strength of the nonlinearity is increased further.

For sufficiently large drought lengths $T$, the maximum in $A_{\min}$ occurs at $\xi = 0$ and thus any $\xi > 0$ reduces the minimum water requirements of the system. The upper bound $A_{\max}$ of the parameter region supporting pattern onset mimics the behaviour of $A_{\min}$. The size of the parameter region in which pattern onset occurs increases slightly with increasing $\xi$, but changes to its size are insignificant compared to changes causes by variations in the interpulse time $T$.

### 4.3. Nonlinear PDEs

The original impulsive model (2.5) is based on the assumption that no plant–water interactions take place during drought periods. The interpulse equations thus form a system of linear and decoupled PDEs that describe linear decay of both plant and water densities between precipitation pulses. We relax this assumption by extending the occurrence of biomass growth into the interpulse phase. This changes the PDE system to

$$\frac{\partial u_n}{\partial t} = -Bu_n + C\left(\frac{u_n}{1+u_n}\right)^2 w_n,$$
$$\frac{\partial w_n}{\partial t} = -w_n - C\left(\frac{u_n}{1+u_n}\right)^2 w_n + d\frac{\partial^2 w_n}{\partial x^2},$$

where the nondimensional constant $C$ accounts for the rate of water uptake. The pulse equations (2.5c) and (2.5d) remain unchanged, i.e. there is still a pulse of plant growth synchronised with a precipitation event.

While a typical estimate is $C = 10$ [86], we use our numerical scheme to investigate how a gradual increase from $C = 0$ (which corresponds to the model studied analytically in Section 3) affects the pattern onset observed in the system. An increase in the plants' growth rate during drought periods causes a decrease in the existence threshold $A_{\min}$ of a spatially uniform non-desert equilibrium and the precipitation level $A_{\max}$ at which pattern onset occurs (Fig. 4.3(b)). This decrease is caused by a reduction in total resource loss through evaporation and the associated increase in water availability to plants. In the original model (2.5)

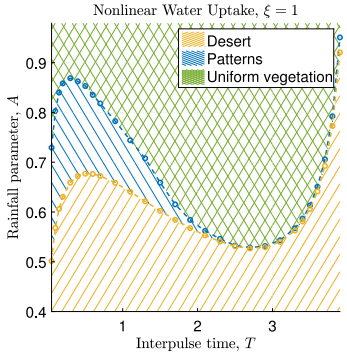


(a) Classification of the $A$-$T$ parameter plane.

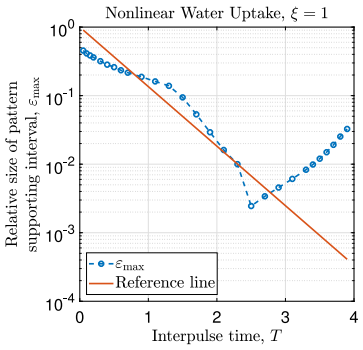


(b) Relative size of the rainfall interval supporting pattern onset.

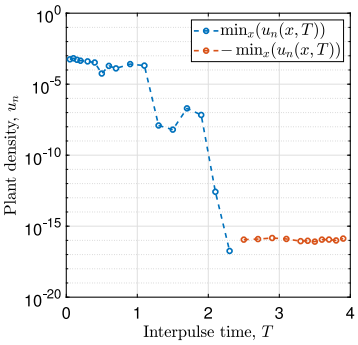


(c) Minimum plant density

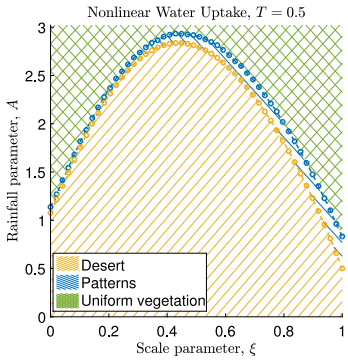


(d) Classification of the $A$-$\xi$ parameter plane.

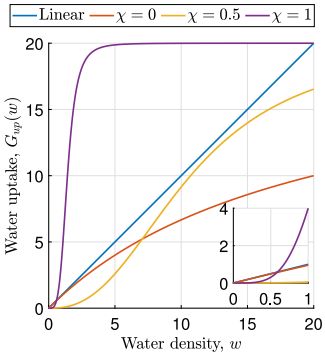


(e) Water uptake functional response.

**Fig. 4.2.** Classification plots for a nonlinear functional response in the water uptake function. The classifications (a) and (d) into states of desert, onset of spatial patterns and uniform vegetation are based on the numerical scheme described in Section 4.1. The transition threshold $A_{\max}$ is determined up to an interval of size $10^{-5}$, the level of $A_{\min}$ up to an interval of size $10^{-8}$. The relative size of $[A_{\min}, A_{\max}]$ corresponding to the classification in (a) is shown in (b), where the reference line is of slope $\exp(-2T)$. The parameter values used in both simulations are $B = 0.45$ and $d = 500$. The water uptake function $G_{\text{up}}(w)$ is shown in (e) for several values of $\xi$, with its behaviour close to the origin shown in the inset. The minimum plant density before a rainfall pulse $\min_{x\in[-x_{\max},x_{\max}]}\{u_n(x,T)\}$ of a stable pattern is shown in (c), where the blue and red markers indicate positive and negative values of $u_n$, respectively. This visualises the numerical issues encountered in simulations for longer interpulse times $T$. (For interpretation of the references to colour in this figure legend, the reader is referred to the web version of this article.)

($C = 0$), water that is not consumed by plants during the rainfall pulse undergoes exponential decay due to evaporation during the interpulse period and is lost from the system. If $C \neq 0$, however, water that enters the drought phase not only evaporates but also continues to be converted into plant biomass, which causes a reduction in evaporation losses.

The second main conclusion arising from the inclusion of a nonlinear coupling of the interpulse PDEs is the conservation of a large parameter region in which pattern onset occurs for large $T$ (Fig. 4.3(a)), instead of an exponential decay of its size with increasing $T$. The existence of such a region is due to the inclusion of a pattern-inducing feedback in the interpulse PDEs. More water is consumed in regions of high biomass density, which causes the homogenising effect of water diffusion to redistribute more water towards these regions yielding further plant growth. If water uptake between pulses is weak (small $C$), or as in the original model non-existent ($C = 0$), the system's only pattern-forming feedback loop consists of the nonlinearity in the plant growth term in the update equations in combination with the homogenising property of water diffusion in the interpulse PDEs. The latter loses its impact as $T$ is increased, as evaporation effects become dominant and cause a decrease in water availability at the end of the interpulse phase. The water density at the growth pulse therefore only depends on the intensity of the rain event, but is independent of the diffusion process that occurs before the rainfall pulse. This weakens the strength of the pattern-inducing feedback loop and causes the decrease in the size of the parameter region in which pattern onset occurs.

### 4.4. Kernel functions

In the linear stability analysis in Section 3.1, we set the plant dispersal kernel to the Laplace kernel (2.3). Seed dispersal behaviour, however, depends both on species and environmental conditions [72]. Similar to the work on a previous model [38], we use our numerical scheme to investigate effects caused by setting the dispersal kernel to the Gaussian

$$\phi(x) = \frac{a_g}{\sqrt{\pi}} e^{-a_g^2 x^2}, \quad a > 0, x \in \mathbb{R}, \tag{4.1}$$

and the power law distribution

$$\phi(x) = \frac{(b-1)a_p}{2\left(1 + a_p|x|\right)^b}, \quad a > 0, b > 3, x \in \mathbb{R}. \tag{4.2}$$

We base our comparison on the kernels' standard deviations, which are given by $\sigma(a) = \sqrt{2}/a$ for the Laplacian kernel (2.3), $\sigma(a_g) = 1/(\sqrt{2}\,a_g)$ for the Gaussian kernel (4.1) and $\sigma(a_p) = \sqrt{2}/(\sqrt{b^2 - 5b + 6}\,a_p)$ for the power law kernel (4.2) provided $b > 3$. It is perfectly reasonable to perform simulations with kernels of infinite standard deviation (e.g. $b < 3$ in the power

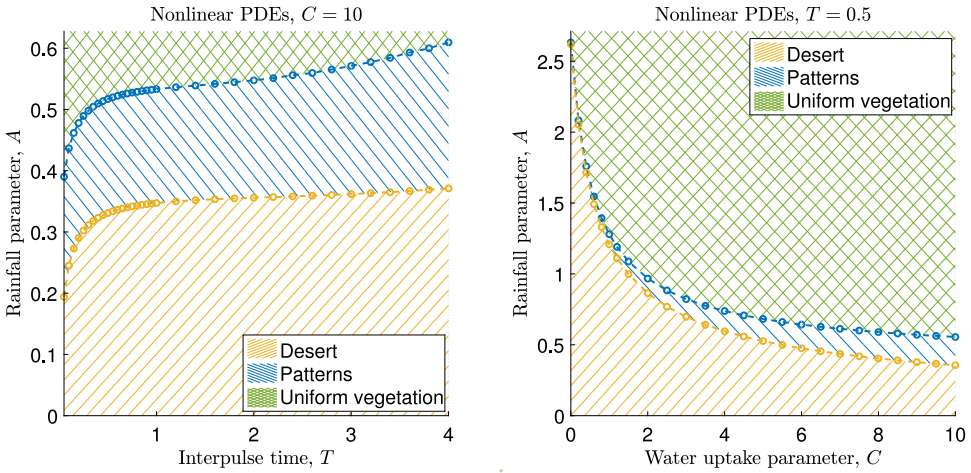


(a) Classification of the $A$-$T$ parameter plane. (b) Classification of the $A$-$C$ parameter plane.

**Fig. 4.3.** Classification plots for the inclusion of plant growth in the interpulse PDEs. The classifications into states of desert, onset of spatial patterns and uniform vegetation is based on the numerical scheme described in Section 4.1. The transition threshold $A_{\max}$ is determined up to an interval of size $10^{-5}$, the level of $A_{\min}$ up to an interval of size $10^{-8}$. The parameter values used in both simulations are $B = 0.45$ and $d = 500$.

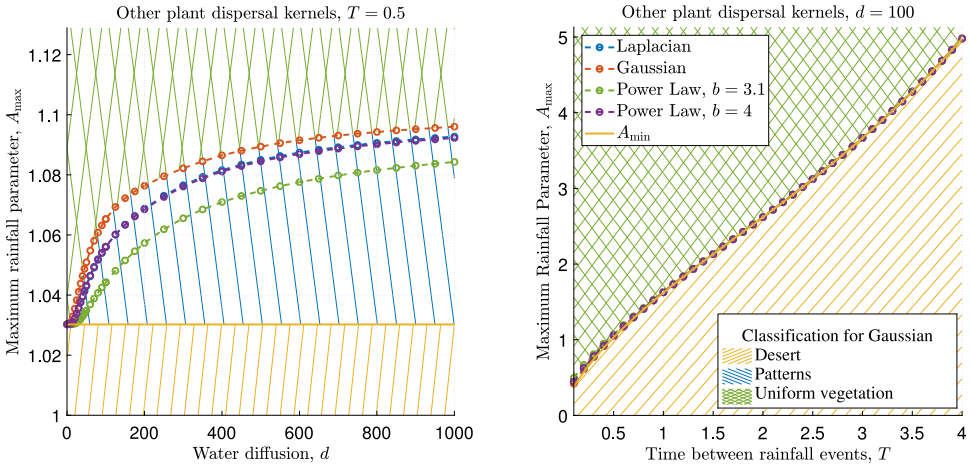


(a) (b)

**Fig. 4.4.** Changes to $A_{\max}$ under variation of water diffusion and the time between rain pulses. This figure visualises changes to the critical rainfall parameter $A_{\max}$ under changes of the water diffusion rate $d$ ((a)) and the interpulse time $T$ ((b)). The rainfall threshold $A_{\max}$ is determined up to an interval of length $10^{-4}$ for $d = \{0, 5, \ldots, 50, 60 \ldots 100, 125, \ldots, 200, 250, \ldots, 1000\}$ and $T = \{0.1, 0.2, \ldots, 4\}$, respectively. Plant mortality is set to $B = 0.45$. The legend applies to both parts of the figure.

law kernel) but in the interest of comparing results for the kernels based on their standard deviation we consider only $b = 3.1$ and $b = 4$.

In the simulations we are interested in both the effects of changes to the shape of the dispersal kernel and the effects caused by a variation in the temporal intermittency of precipitation. As shown in Fig. 4.4(b), the latter bears much more influence on the rainfall threshold $A_{\max}$ than the choice of plant dispersal kernel. Indeed, the results obtained for all kernel functions follow the narrow band of exponentially decaying size in the $T - A$ parameter region in which pattern existence has been shown for the Laplace kernel in Section 3.1 and in particular in Fig. 3.2(a).

While the effects of the kernel shape are negligible compared to changes of the interpulse time $T$, their influence on the system can still be studied if $T$ is fixed. Instead of varying $T$, we opt to investigate how the threshold $A_{\max}$, at which patterns cease to exist, changes under variations of the water diffusion coefficient $d$. This allows us to draw a connection to the results of the linear stability analysis visualised in Fig. 3.1. Our numerical scheme shows that all kernel functions considered in the simulations qualitatively follow the same behaviour, which agrees with the analytically deduced result for the Laplace kernel in Section 3.1. For sufficiently low levels of rainfall, the diffusion coefficient needs to exceed a threshold to give rise to an instability resulting in the onset of spatial patterns. There does, however, exist an upper bound (not shown in Fig. 4.4(a)) on the rainfall parameter for each kernel function above which pattern onset from a perturbation of the steady state is impossible. Due to the nondimensionalisation of the model an increase in the diffusion coefficient $d$ corresponds to a decrease in the width of the dispersal kernels. Thus, for a fixed kernel function an increase in kernel width inhibits the onset of patterns. Note, however, that information on the kernels' standard deviation, which we use as a measurement of kernel width, is insufficient to make comparisons between results for different kernel functions. Conditions for pattern onset also depend on the dispersal kernel's type of decay at infinity; for example $A_{\max}$ for

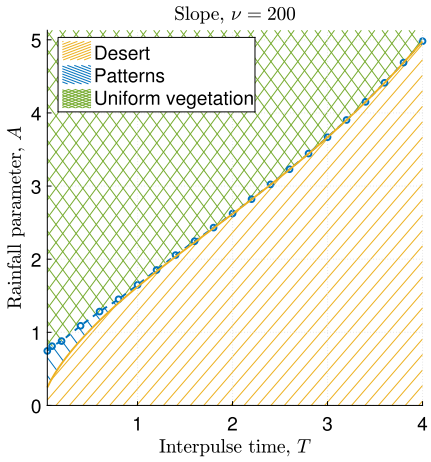


(a) Classification of the $A$-$T$ parameter plane.

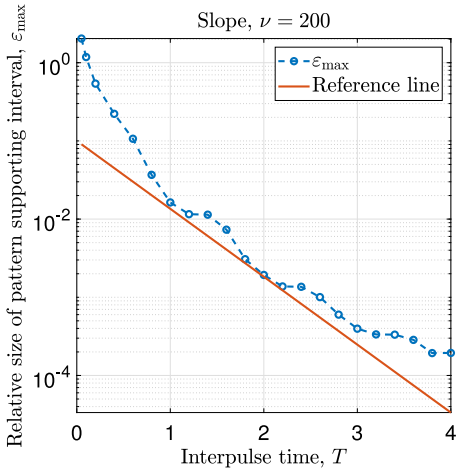


(b) Relative size of the rainfall interval supporting pattern onset.

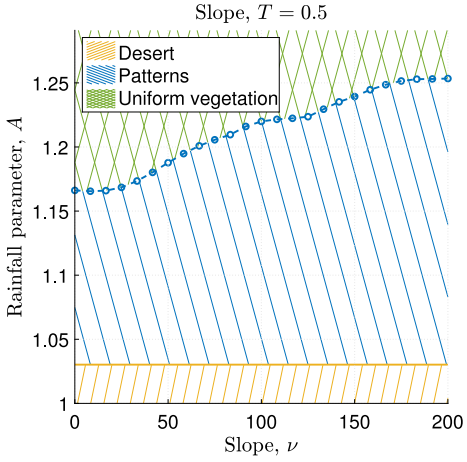


(c) Classification of the $A$-$\nu$ parameter plane.

**Fig. 4.5.** Classification plots for the model on a slope. The classifications into states of desert, onset of spatial patterns and uniform vegetation are based on the numerical scheme described in Section 4.1. The transition threshold $A_{\max}$ is determined up to an interval of size $10^{-8}$, the level of $A_{\min}$ is given by (3.3). The relative size of $[A_{\min}, A_{\max}]$ is shown in (b), where the reference line has slope $\exp(-2T)$. The parameter values used in both simulations are $B = 0.45$ and $d = 500$.

the Laplace kernel and the power law kernel with $b = 4$ coincide in Fig. 4.4(a), even though their standard deviations are $\sigma_L = \sqrt{2}$ and $\sigma_P = 1$, respectively.

### 4.5. Slope

Finally, we lift the restriction of the flat spatial domain for which the linear stability analysis of (2.5) was performed in Section 3. Originally, the Klausmeier model was proposed to describe vegetation bands on sloped terrain and a lot of previous work has focused on this scenario (e.g. [27,34,38]). A numerical investigation into the existence of spatial patterns of (2.5) on a sloped spatial domain shows that the threshold $A_{\max}$ at which a transition between uniform and patterned vegetation occurs, increases with increasing slope $\nu$ (Fig. 4.5(c)). The lower bound $A_{\min}$ of the parameter region supporting the onset of spatial patterns from spatially nonuniform perturbations of the equilibrium, is a non-spatial property and thus independent of the slope parameter $\nu$. Thus the size of $[A_{\min}, A_{\max}]$ increases with increasing $\nu$. Ecologically, this stems from an increase in the strength of the pattern-forming mechanism. On steeper slopes water flows downhill faster and thus increases the competitive advantage of existing biomass patches.

This increase in the size of $[A_{\min}, A_{\max}]$ is, however, negligible compared to the decay of the interval's size for increasing interpulse time $T$ (Figs. 4.5(a) and 4.5(b)). Our results indicate that the interval's size decays exponentially, similar to the analytically obtained result (Corollary 3.5) for the model on flat ground in the limit $d \to \infty$. We thus conclude that the simplified model ($\nu = 0$) qualitatively yields the same results on the onset of patterns under variations in the length of the drought period $T$.

## 5. Discussion

In this paper we consider a new impulsive-type model to investigate the effects of rainfall intermittency on the onset of vegetation patterns in semi-arid environments. Most significantly, our results suggest that the decay-type behaviour which dominates during long drought periods inhibits the onset of spatial patterns and that ecosystems benefit from precipitation intermittency if plant species are unable to efficiently use low soil moisture levels.

The inhibition of patterns by low frequency rain events is quantified by the small size of the interval of rainfall levels in which pattern onset occurs. Therefore, plants are able to form a uniform vegetation cover for rainfall levels very close to the

minimum required for the corresponding spatially uniform equilibrium to exist. This pattern-inhibitory effect in the impulsive model (see Corollary 3.5 and Figs. 3.2 and 4.4(b)) can be explained by the weakening effect of the temporal separation of rainfall pulses on the plant growth-water redistribution feedback which is the main contributor in the formation of patterns [1,90]. This positive feedback loop consists of two processes; the increased water utilisation in regions of high biomass and the redistribution of water. In (2.5) these processes occur in different stages. The soil modification by plants affects water consumption and plant growth which only occur in the update equations associated with a rainfall pulse, while water diffusion is accounted for in the interpulse PDE system. Therefore, if plants are in a patterned state, the water density immediately after a rainfall pulse is in antiphase to the plant density (i.e. high water density in regions of low biomass and vice versa). The homogenising property of diffusion thus redistributes water from patches of low biomass to regions where plant density is high. If, however, the separation of precipitation pulses is too long, this homogenising effect loses its impact as water evaporation becomes the dominant process. In the model extension which assumes that plant growth occurs in both the pulse stage and during the interpulse period (Section 4.3), the temporal separation of rainfall events does not weaken the pattern-inducing feedback. The closure of the feedback loop in the interpulse PDEs allows for more water transported to regions of high biomass during drought periods to be utilised and thus supports the pattern-forming mechanism.

For a fixed interpulse time $T$, the reduction in water evaporation associated with this increase in water to biomass conversion causes a reduction in the minimum amount of precipitation required for a spatially uniform equilibrium to exist. We use this minimum on the rainfall parameter ($A_{\min}$) as a proxy for the minimum water requirements of the ecosystem, but emphasise the fact that spatially non-uniform stable states with non-zero plant densities are likely to exist for lower precipitation levels and no information on the resilience of the ecosystem can be extracted from the analysis presented in this paper. For both the extension with nonlinear interpulse PDEs and the original model (2.5), the threshold $A_{\min}$ increases with the drought period length $T$, which indicates that an increase in the time between rainfall events has a detrimental effect on the ecosystem. Even though this does not agree with the majority of reported field observations [54,56], there exists evidence of this inhibitory effect for some dryland species, with an increase in seeds germination rates, a decrease in emergence rates and an increase in seedling mortalities under longer periods of droughts [55,91]. This suggests that an ecosystem's response to temporal variability in precipitation is highly species-dependent and it is important to understand a species' response to oscillations in soil moisture to model its dynamics. Indeed, we have established that changes to the plants' water uptake functional response to the water density (Section 4.2) can reverse the increasing behaviour of the minimum water requirement proxy $A_{\min}$ observed in the original model in which the functional response is linear (Fig. 3.2(a)). If species in an ecosystem remain dormant under low soil moisture levels caused by a high frequency–low intensity rainfall regime, then rainfall intermittency and the associated temporal increases in soil moisture can have a positive impact on the ecosystem [54, 56]. Mathematically, we used a Holling type III functional response to model this dormant behaviour under low soil moisture levels. If the concave-up shape of this species-dependent functional response is sufficiently strong for low water densities, then $A_{\min}$ attains a minimum for an intermediate interpulse time $T$ because water uptake is maximised under such conditions. This is in agreement with results obtained for the Gilad [26] model [61].

The dominant role of precipitation intermittency on the onset of patterns also manifests itself in the fact that, unlike in the Klausmeier models, diffusion alone is insufficient to cause pattern onset in the impulsive model. The onset of spatial patterns still requires the diffusion coefficient to exceed a threshold (Proposition 3.6) but in stark contrast to the Klausmeier models in which a sufficiently large level of diffusion can cause an instability for an arbitrarily large level of rainfall, the effects of diffusion are limited to a small interval of the rainfall parameter (Proposition 3.4), whose size decreases exponentially as precipitation pulses become more infrequent (Corollary 3.5). This deviation form the classical case of a diffusion-driven instability is due to the previously discussed temporal separation of the components of the pattern-inducing feedback that renders diffusion effects insignificant under long drought spells. This property is specific to the system considered in this paper and no generalisations can be made. Indeed, diffusion-driven instabilities have been shown to occur in other impulsive models [67].

A second key aspect of this paper is the effects caused by changes to the width and shape of the plant dispersal kernel. Contrary to the beneficial effect associated with the inhibition of pattern onset due to wide plant dispersal kernels shown by the model in this paper (Fig. 4.4(a)), plants in semi-arid regions are observed to establish narrow dispersal kernels [92]. This is, however, only a secondary effect caused by other adaptations such as protection from seed predators, that are not accounted for in these models but nevertheless affect the vegetation's evolution in arid regions [92]. The quantitatively small changes to the rainfall threshold $A_{\max}$ in the impulsive model are caused by the fact that in the impulsive model only the newly added biomass is dispersed, while in the other models the whole plant density undergoes dispersal. Combined with the claim that plants compensate for the negative effect of a narrow seed dispersal kernel by changes of traits not included in this model, this suggests the combination of the weak response of the impulsive model to changes in the width of the dispersal kernel and the stronger effect of rainfall intermittency provides a more realistic framework than a previous model in which the seed dispersal distance played an important role in the absence of any pulse-type events [38].

To facilitate the mathematical analysis presented in this paper we have opted for a fully deterministic modelling of precipitation. The assumption that rainfall events occur periodically in time and are all of the same intensity is, however, an inaccurate description of the inherently stochastic nature of this key process. A more realistic description of such precipitation events can be achieved through a Poisson process with exponentially distributed rainfall intensities [79]. The model framework presented in this model is, however, insufficient to consider any stochasticity in the rainfall regime. Neither the original model (2.5) nor any of its extensions presented in Section 4 include mechanisms that allow plants to recover from a very low density. Thus, the eventual occurrence of a long drought period (possibly combined with low intensity pulses) under a stochastic precipitation regime inevitably causes the extinction of plants in the long term. In reality, plants have developed mechanisms such as seed dormancy that allow recovery from low biomass densities [91]. Their inclusion in a mathematical model is required to better understand an ecosystem's response to stochasticity in environmental conditions. Nevertheless, it is possible to relate the results of the deterministic model presented in this paper to a stochastic setting. Similar to a previous study of effects of temporal variations of rainfall pulses on dryland ecosystems, the constants involved in the deterministic modelling of precipitation can be seen as the expected values that arise from the underlying stochastic processes [60]. If this assumption is applied then our results on thresholds such as $A_{\max}$ present an approximation to

the expectations of the respective quantities when any higher order moments (variance, etc.) of the random variables associated with the description of precipitation are neglected [60].

While the model extensions (and possibly combinations thereof) presented in Section 4 provide a more realistic description of the ecosystem dynamics under a pulse type precipitation regime, the analytical study of the simpler model (2.5) in Section 3 is an important tool to gain a better understanding of vegetation patterns in semi-arid environments. Numerical approaches tend to become unreliable as the length of the drought periods increases because decay-type processes of long dry spells reduce the plant density in troughs of the spatial pattern to very small values. This makes numerical integration techniques error-prone and emphasises the importance of analytical pathways into the problem (Fig. 4.2(c)).

The results presented in this paper are based on our analysis of a theoretical model and a comparison with empirical data would be desirable to test these hypotheses. Daily rainfall data is available from the 1980s to the present (see e.g. [93] for data from Africa), and data with a coarser temporal scale dates back to the 1940s [94]. However, obtaining high-quality data for vegetation in dryland ecosystems is notoriously difficult due to the large spatial and temporal scales of the ecosystem dynamics. Some limited data obtained from satellite images exists (e.g. [7]), for example on wavelength which can be used as a proxy for biomass, but a comparison with any model predictions would require a better measure of key ecological properties, as well as a long time series of data points.

In this paper, we have analysed the effects of rainfall intermittency on pattern onset in dryland vegetation in one space dimension only. On flat ground in particular, the consideration of a two-dimensional domain would be a natural extension. This could provide more insight into the patterns' properties such as its type (gap pattern, labyrinth pattern, stripes or spots) under changes to the precipitation regime [95]. The analysis of the impulsive model on a two-dimensional domain would be significantly more challenging, but methods for studying pattern formation in PDEs on such domains exist (see, for example, [96] for an analysis of the Klausmeier model), which hold the potential to be adapted to the framework of an impulsive model.

A further natural area of potential future work could involve an accurate description of overland water flow during a rainfall event. For sloped terrain such a description has been provided and applied to a mathematical model describing the evolution of vegetation patterns by Siteur et al. [60]. Their argument is based on water instantaneously flowing downhill and infiltrating the soil in areas of high biomass and can thus not be applied to a flat spatial domain. Indeed, overland flow of water during intense rainfall events on semi-arid flat plains is the subject of ongoing research (e.g. [83–85]). A detailed description of the overland water flow and infiltration into the soil that occurs before water is consumed by plants relies on a clear distinction between the surface water density and the soil moisture. Such a separation is used in alternative model frameworks [25,26,82], which could be utilised to include the description of water redistribution during rainfall events under a pulse-type precipitation regime.

The model introduced in this paper is based on the Klausmeier model, which is a model that is deliberately kept simple to facilitate a mathematical analysis of it. A number of more complex models exist (see [78,97,98] for reviews) that study different aspects of patterned vegetation in more detail by, for example, including two coexisting plant species [39,73,75,99], describing water uptake as a nonlocal process [26,86] or considering effects of nonlocal grazing [100,101]. For some of these models numerical studies have investigated the effects of temporal rainfall variability [59–61] and an analytical analysis of those models similar to the work done in this paper could provide further insight how pulse-type phenomena affect patterns in semi-arid environments.

## CRediT authorship contribution statement

**L. Eigentler:** Conceptualization, Methodology, Formal analysis, Writing - original draft, Writing - review & editing, Visualization. **J.A. Sherratt:** Conceptualization, Methodology, Writing - review & editing.

## Acknowledgements

Lukas Eigentler was supported by The Maxwell Institute Graduate School, United Kingdom in Analysis and its Applications, a Centre for Doctoral Training funded by the UK Engineering and Physical Sciences Research Council (grant EP/L016508/01), the Scottish Funding Council, United Kingdom, Heriot-Watt University, United Kingdom and the University of Edinburgh, United Kingdom.

## References

[1] M. Rietkerk, J. van de Koppel, Regular pattern formation in real ecosystems, Trends Ecol. Evol. 23 (3) (2008) 169–175, http://dx.doi.org/10.1016/j.tree.2007.10.013.

[2] E. Meron, Pattern formation - A missing link in the study of ecosystem response to environmental changes, Math. Biosci. 271 (2016) 1–18, http://dx.doi.org/10.1016/j.mbs.2015.10.015.

[3] W.A. Macfadyen, Vegetation patterns in the semi-desert plains of british somaliland, Geograph. J. 116 (4/6) (1950) 199–211, http://dx.doi.org/10.2307/1789384.

[4] C. Valentin, J. d'Herbés, J. Poesen, Soil and water components of banded vegetation patterns, CATENA 37 (1–2) (1999) 1–24, http://dx.doi.org/10.1016/S0341-8162(99)00053-3.

[5] P. Gandhi, S. Iams, S. Bonetti, M. Silber, Vegetation Pattern Formation in Drylands, in: Dryland Ecohydrology, Springer International Publishing, 2019, pp. 469–509, http://dx.doi.org/10.1007/978-3-030-23269-6_18.

[6] J. Müller, Floristic and structural pattern and current distribution of tiger bush vegetation in Burkina Faso (West Africa), assessed by means of belt transects and spatial analysis, Appl. Ecol. Environ. Res. 11 (2013) 153–171, http://dx.doi.org/10.15666/aeer/1102_153171.

[7] V. Deblauwe, P. Couteron, J. Bogaert, N. Barbier, Determinants and dynamics of banded vegetation pattern migration in arid climates, Ecol. Monogr. 82 (1) (2012) 3–21, http://dx.doi.org/10.1890/11-0362.1.

[8] C.F. Hemming, Vegetation arcs in Somaliland, J. Ecol. 53 (1) (1965) 57–67, http://dx.doi.org/10.2307/2257565.

[9] K. Gowda, S. Iams, M. Silber, Signatures of human impact on self-organized vegetation in the Horn of Africa, Sci. Rep. 8 (2018) 1–8, http://dx.doi.org/10.1038/s41598-018-22075-5.

[10] D. Dunkerley, K. Brown, Oblique vegetation banding in the Australian arid zone: implications for theories of pattern evolution and maintenance, J. Arid. Environ. 51 (2) (2002) 163–181, http://dx.doi.org/10.1006/jare.2001.0940.

[11] M.M. las Heras, P.M. Saco, G.R. Willgoose, D.J. Tongway, Variations in hydrological connectivity of Australian semiarid landscapes indicate abrupt changes in rainfall-use efficiency of vegetation, J. Geophys. Res. G: Biogeosci. 117 (2012) G03009, http://dx.doi.org/10.1029/2011JG001839.

[12] E. Sheffer, J. Hardenberg, H. Yizhaq, M. Shachak, E. Meron, B. Blasius, Emerged or imposed: a theory on the role of physical templates and self-organisation for vegetation patchiness, Ecol. Lett. 16 (2) (2013) 127–139, http://dx.doi.org/10.1111/ele.12027.

[13] E. Buis, A. Veldkamp, B. Boeken, N. van Breemen, Controls on plant functional surface cover types along a precipitation gradient in the Negev Desert of Israel, J. Arid. Environ. 73 (1) (2009) 82–90, http://dx.doi.org/10.1016/j.jaridenv.2008.09.008.

[14] G.G. Penny, K.E. Daniels, S.E. Thompson, Local properties of patterned vegetation: quantifying endogenous and exogenous effects, Philos. Trans. R. Soc. London, Ser. A 371 (2013) 20120359, http://dx.doi.org/10.1098/rsta.2012.0359.

[15] J.D. Pelletier, S.B. DeLong, C.A. Orem, P. Becerra, K. Compton, K. Gressett, J. Lyons-Baral, L.A. McGuire, J.L. Molaro, J.C. Spinler, How do vegetation bands form in dry lands? Insights from numerical modeling and field studies in southern Nevada, USA, J. Geophys. Res. F: Earth Surface 117:F04026 (2012) http://dx.doi.org/10.1029/2012JF002465.
[16] C. Fernandez-Oto, D. Escaff, J. Cisternas, Spiral vegetation patterns in high-altitude wetlands, Ecol. Complexity 37 (2019) 38–46, http://dx.doi.org/10.1016/j.ecocom.2018.12.003.
[17] S. Kéfi, M. Rietkerk, C.L. Alados, Y. Pueyo, V. Papanastasis, A. ElAich, P. de Ruiter, Spatial vegetation patterns and imminent desertification in Mediterranean arid ecosystems, Nature 449 (7159) (2007) 213–217, http://dx.doi.org/10.1038/nature06111.
[18] M. Rietkerk, S.C. Dekker, P.C. de Ruiter, J. van de Koppel, Self-organized patchiness and catastrophic shifts in ecosystems, Science 305 (5692) (2004) 1926–1929, http://dx.doi.org/10.1126/science.1101867.
[19] R. Corrado, A.M. Cherubini, C. Pennetta, Early warning signals of desertification transitions in semiarid ecosystems, Phys. Rev. E (3) 90 (2014) 062705, http://dx.doi.org/10.1103/PhysRevE.90.062705.
[20] K. Gowda, Y. Chen, S. Iams, M. Silber, Assessing the robustness of spatial pattern sequences in a dryland vegetation model, Proc. R. Soc. Lond. Ser. A Math. Phys. Eng. Sci. 472 (2016) 20150893, http://dx.doi.org/10.1098/rspa.2015.0893.
[21] E. Meron, From patterns to function in living systems: Dryland ecosystems as a case study, Annu. Rev. Condens. Matter Phys. 9 (1) (2018) 79–103, http://dx.doi.org/10.1146/annurev-conmatphys-033117-053959.
[22] V. Dakos, S. Kéfi, M. Rietkerk, E.H. van Nes, M. Scheffer, Slowing down in spatially patterned ecosystems at the brink of collapse, Am. Nat. 177 (6) (2011) E153–E166, http://dx.doi.org/10.1086/659945.
[23] P.M. Saco, M. Moreno-de las Heras, S. Keesstra, J. Baartman, O. Yetemen, J.F. Rodriguez, Vegetation and soil degradation in drylands: Non linear feedbacks and early warning signals, Curr. Opin. Environ. Sci. Health 5 (2018) 67–72, http://dx.doi.org/10.1016/j.coesh.2018.06.001.
[24] Y.R. Zelnik, P. Gandhi, E. Knobloch, E. Meron, Implications of tristability in pattern-forming ecosystems, Chaos 28 (3) (2018) 033609, http://dx.doi.org/10.1063/1.5018925.
[25] M. Rietkerk, M.C. Boerlijst, F. van Langevelde, R. HilleRisLambers, J. van de Koppel, L. Kumar, H.H.T. Prins, A.M. de Roos, Self-organization of vegetation in arid ecosystems, Am. Nat. 160 (4) (2002) 524–530, http://dx.doi.org/10.1086/342078.
[26] E. Gilad, J. von Hardenberg, A. Provenzale, M. Shachak, E. Meron, Ecosystem engineers: From pattern formation to habitat creation, Phys. Rev. Lett. 93 (2004) 098105, http://dx.doi.org/10.1103/PhysRevLett.93.098105.
[27] C.A. Klausmeier, Regular and irregular patterns in semiarid vegetation, Science 284 (5421) (1999) 1826–1828, http://dx.doi.org/10.1126/science.284.5421.1826.
[28] J.J.R. Bennett, J.A. Sherratt, Long-distance seed dispersal affects the resilience of banded vegetation patterns in semi-deserts, J. Theoret. Biol. 481 (2018) 151–161, http://dx.doi.org/10.1016/j.jtbi.2018.10.002.
[29] J.A. Sherratt, An analysis of vegetation stripe formation in semi-arid landscapes, J. Math. Biol. 51 (2) (2005) 183–197, http://dx.doi.org/10.1007/s00285-005-0319-5.
[30] J.A. Sherratt, G.J. Lord, Nonlinear dynamics and pattern bifurcations in a model for vegetation stripes in semi-arid environments, Theor. Popul. Biol. 71 (1) (2007) 1–11, http://dx.doi.org/10.1016/j.tpb.2006.07.009.
[31] J.A. Sherratt, Pattern solutions of the klausmeier model for banded vegetation in semi-arid environments I, Nonlinearity 23 (10) (2010) 2657–2675, http://dx.doi.org/10.1088/0951-7715/23/10/016.
[32] J.A. Sherratt, Pattern solutions of the Klausmeier model for banded vegetation in semi-arid environments II: patterns with the largest possible propagation speeds, Proc. R. Soc. Lond. Ser. A Math. Phys. Eng. Sci. 467 (2135) (2011) 3272–3294, http://dx.doi.org/10.1098/rspa.2011.0194.
[33] J.A. Sherratt, Pattern solutions of the Klausmeier model for banded vegetation in semi-arid environments III: The transition between homoclinic solutions, Physica D 242 (1) (2013) 30–41, http://dx.doi.org/10.1016/j.physd.2012.08.014.
[34] J.A. Sherratt, Pattern solutions of the Klausmeier model for banded vegetation in semiarid environments IV: Slowly moving patterns and their stability, SIAM J. Appl. Math. 73 (1) (2013) 330–350, http://dx.doi.org/10.1137/120862648.
[35] J.A. Sherratt, Pattern solutions of the Klausmeier model for banded vegetation in semiarid environments V: The transition from patterns to desert, SIAM J. Appl. Math. 73 (4) (2013) 1347–1367, http://dx.doi.org/10.1137/120899510.
[36] K. Siteur, E. Siero, M.B. Eppinga, J.D. Rademacher, A. Doelman, M. Rietkerk, Beyond Turing: The response of patterned ecosystems to environmental change, Ecol. Complexity 20 (2014) 81–96, http://dx.doi.org/10.1016/j.ecocom.2014.09.002.
[37] N. Ursino, S. Contarini, Stability of banded vegetation patterns under seasonal rainfall and limited soil moisture storage capacity, Adv. Water Resour. 29 (10) (2006) 1556–1564, http://dx.doi.org/10.1016/j.advwatres.2005.11.006.
[38] L. Eigentler, J.A. Sherratt, Analysis of a model for banded vegetation patterns in semi-arid environments with nonlocal dispersal, J. Math. Biol. 77 (3) (2018) 739–763, http://dx.doi.org/10.1007/s00285-018-1233-y.
[39] L. Eigentler, J.A. Sherratt, Metastability as a coexistence mechanism in a model for dryland vegetation patterns, Bull. Math. Biol. 81 (7) (2019) 2290–2322, http://dx.doi.org/10.1007/s11538-019-00606-z, https://doi.org/10.1007/s11538-019-00606-z.
[40] X. Wang, G. Zhang, The influence of infiltration feedback on the characteristic of banded vegetation pattern on hillsides of semiarid area, PLoS One 14 (1) (2019) e0205715, http://dx.doi.org/10.1371/journal.pone.0205715.
[41] X. Wang, G. Zhang, Vegetation pattern formation in seminal systems due to internal competition reaction between plants, J. Theoret. Biol. 458 (2018) 10–14, http://dx.doi.org/10.1016/j.jtbi.2018.08.043.
[42] G. Consolo, C. Currò, G. Valenti, Supercritical and subcritical Turing pattern formation in a hyperbolic vegetation model for flat arid environments, Physica D 398 (2019) 141–163, http://dx.doi.org/10.1016/j.physd.2019.03.006.
[43] G. Consolo, G. Valenti, Secondary seed dispersal in the Klausmeier model of vegetation for sloped semi-arid environments, Ecol. Modell. 402 (2019) 66–75, http://dx.doi.org/10.1016/j.ecolmodel.2019.02.009.
[44] A. Marasco, A. Iuorio, F. Carteni, G. Bonanomi, D.M. Tartakovsky, S. Mazzoleni, F. Giannino, Vegetation pattern formation due to interactions between water availability and toxicity in plant–soil feedback, Bull. Math. Biol. 76 (11) (2014) 2866–2883, http://dx.doi.org/10.1007/s11538-014-0036-6.
[45] R. Bastiaansen, O. Jaïbi, V. Deblauwe, M.B. Eppinga, K. Siteur, E. Siero, S. Mermoz, A. Bouvet, A. Doelman, M. Rietkerk, Multistability of model and real dryland ecosystems through spatial self-organization, Proc. Natl. Acad. Sci. (2018) 11256–11261, http://dx.doi.org/10.1073/pnas.1804771115.
[46] L. Eigentler, J.A. Sherratt, An integrodifference model for vegetation patterns in semi-arid environments with seasonality, 2019, arXiv:http://arxiv.org/abs/1911.10964.
[47] L. Eigentler, J.A. Sherratt, Spatial self-organisation enables species coexistence in a model for savanna ecosystems, J. Theoret. Biol. 487 (2020) 110122, http://dx.doi.org/10.1016/j.jtbi.2019.110122.
[48] I. Noy-Meir, Desert ecosystems: Environment and producers, Annu. Rev. Ecol. Syst. 4 (1973) 25–51, http://dx.doi.org/10.1146/annurev.es.04.110173.000325.
[49] T. Navarro, V. Pascual, C. Alados, B. Cabezudo, Growth forms, dispersal strategies and taxonomic spectrum in a semi-arid shrubland in SE Spain, J. Arid. Environ. 73 (1) (2009) 103–112, http://dx.doi.org/10.1016/j.jaridenv.2008.09.009.
[50] K. van Rheede van Oudtshoorn, M.W. van Rooyen, Dispersal Biology of Desert Plants, in: Adaptations of Desert Organisms, Springer, Berlin Heidelberg, 2013.
[51] A. Fravolini, K.R. Hultine, E. Brugnoli, R. Gazal, N.B. English, D.G. Williams, Precipitation pulse use by an invasive woody legume: the role of soil texture and pulse size, Oecologia 144 (4) (2005) 618–627, http://dx.doi.org/10.1007/s00442-005-0078-4.
[52] Y. Fan, X. Li, X. Wu, L. Li, W. Li, Y. Huang, Divergent responses of vegetation aboveground net primary productivity to rainfall pulses in the Inner Mongolian Plateau, China, J. Arid. Environ. 129 (2016) 1–8, http://dx.doi.org/10.1016/j.jaridenv.2016.02.002.
[53] B. Liu, W.Z. Zhao, Z.J. Wen, Photosynthetic response of two shrubs to rainfall pulses in desert regions of northwestern China, Photosynthetica 50 (1) (2012) 109–119, http://dx.doi.org/10.1007/s11099-012-0015-9.
[54] J.L. Heisler-White, A.K. Knapp, E.F. Kelly, Increasing precipitation event size increases aboveground net primary productivity in a semi-arid grassland, Oecologia 158 (1) (2008) 129–140, http://dx.doi.org/10.1007/s00442-008-1116-9.
[55] J.T. Lundholm, D.W. Larson, Experimental separation of resource quantity from temporal variability: seedling responses to water pulses, Oecologia 141 (2) (2004) 346–352, http://dx.doi.org/10.1007/s00442-003-1454-6.
[56] A.A. Sher, D.E. Goldberg, A. Novoplansky, The effect of mean and variance in resource supply on survival of annuals from mediterranean and desert environments, Oecologia 141 (2) (2004) 353–362, http://dx.doi.org/10.1007/s00442-003-1435-9.
[57] IPCC, 2014, in: Core Writing Team, R. Pachauri, L. Meyer (Eds.), Climate Change 2014: Synthesis Report. Contribution of Working Groups I, II and III to the Fifth Assessment Report of the Intergovernmental Panel on Climate Change, IPCC, Geneva, Switzerland, 2014.

[58] D.R. Easterling, G.A. Meehl, C. Parmesan, S.A. Changnon, T.R. Karl, L.O. Mearns, Climate extremes: Observations, modeling, and impacts, Science 289 (5487) (2000) 2068–2074, http://dx.doi.org/10.1126/science.289.5487.2068.

[59] V. Guttal, C. Jayaprakash, Self-organization and productivity in semi-arid ecosystems: implications of seasonality in rainfall, J. Theoret. Biol. 248 (3) (2007) 490–500, http://dx.doi.org/10.1016/j.jtbi.2007.05.020.

[60] K. Siteur, M.B. Eppinga, D. Karssenberg, M. Baudena, M.F. Bierkens, M. Rietkerk, How will increases in rainfall intensity affect semiarid ecosystems? Water Resour. Res. 50 (7) (2014) 5980–6001, http://dx.doi.org/10.1002/2013wr014955.

[61] A. Kletter, J. von Hardenberg, E. Meron, A. Provenzale, Patterned vegetation and rainfall intermittency, J. Theoret. Biol. 256 (4) (2009) 574–583, http://dx.doi.org/10.1016/j.jtbi.2008.10.020.

[62] M. Baudena, G. Boni, L. Ferraris, J. von Hardenberg, A. Provenzale, Vegetation response to rainfall intermittency in drylands: Results from a simple ecohydrological box model, Adv. Water Resour. 30 (5) (2007) 1320–1328, http://dx.doi.org/10.1016/j.advwatres.2006.11.006.

[63] M. Baudena, A. Provenzale, Rainfall intermittency and vegetation feedbacks in drylands, Hydrol. Earth Syst. Sci. 12 (2) (2008) 679–689, http://dx.doi.org/10.5194/hess-12-679-2008.

[64] F. Laio, A. Porporato, L. Ridolfi, I. Rodriguez-Iturbe, Plants in water-controlled ecosystems: active role in hydrologic processes and response to water stress: II. Probabilistic soil moisture dynamics, Adv. Water Resour. 24 (7) (2001) 707–723, http://dx.doi.org/10.1016/S0309-1708(01)00005-7.

[65] O. Vasilyeva, F. Lutscher, M. Lewis, Analysis of spread and persistence for stream insects with winged adult stages, J. Math. Biol. 72 (4) (2016) 851–875, http://dx.doi.org/10.1007/s00285-015-0932-x.

[66] Q. Huang, H. Wang, M.A. Lewis, A hybrid continuous/discrete-time model for invasion dynamics of zebra mussels in rivers, SIAM J. Appl. Math. 77 (3) (2017) 854–880, http://dx.doi.org/10.1137/16m1057826.

[67] X. Wang, F. Lutscher, Turing patterns in a predator–prey model with seasonality, J. Math. Biol. 78 (3) (2018) 711–737, http://dx.doi.org/10.1007/s00285-018-1289-8.

[68] M. Akhmet, M. Beklioglu, T. Ergenc, V. Tkachenko, An impulsive ratio-dependent predator–prey system with diffusion, Nonlinear Anal. RWA 7 (5) (2006) 1255–1267, http://dx.doi.org/10.1016/j.nonrwa.2005.11.007.

[69] E. Pachepsky, R.M. Nisbet, W.W. Murdoch, Between discrete and continuous: Consumer–resource dynamics with synchronised reproduction, Ecology 89 (1) (2008) 280–288, http://dx.doi.org/10.1890/07-0641.1.

[70] M. Lewis, B. Li, Spreading speed, traveling waves, and minimal domain size in impulsive reaction–diffusion models, Bull. Math. Biol. 74 (10) (2012) 2383–2402, http://dx.doi.org/10.1007/s11538-012-9757-6.

[71] S.A. Geritz, E. Kisdi, On the mechanistic underpinning of discrete-time population models with complex dynamics, J. Theoret. Biol. 228 (2) (2004) 261–269, http://dx.doi.org/10.1016/j.jtbi.2004.01.003.

[72] J.M. Bullock, L.M. González, R. Tamme, L. Götzenberger, S.M. White, M. Pärtel, D.A.P. Hooftman, A synthesis of empirical plant dispersal kernels, J. Ecol. 105 (1) (2017) 6–19, http://dx.doi.org/10.1111/1365-2745.12666.

[73] M. Baudena, M. Rietkerk, Complexity and coexistence in a simple spatial model for arid savanna ecosystems, Theor. Ecol. 6 (2) (2013) 131–141, http://dx.doi.org/10.1007/s12080-012-0165-1.

[74] Y. Pueyo, S. Kéfi, C.L. Alados, M. Rietkerk, Dispersal strategies and spatial organization of vegetation in arid ecosystems, Oikos 117 (10) (2008) 1522–1532, http://dx.doi.org/10.1111/j.0030-1299.2008.16735.x.

[75] Y. Pueyo, S. Kéfi, R. Díaz-Sierra, C. Alados, M. Rietkerk, The role of reproductive plant traits and biotic interactions in the dynamics of semi-arid plant communities, Theor. Popul. Biol. 78 (4) (2010) 289–297, http://dx.doi.org/10.1016/j.tpb.2010.09.001.

[76] B.J. Kealy, D.J. Wollkind, A nonlinear stability analysis of vegetative Turing pattern formation for an interaction–diffusion plant-surface water model system in an arid flat environment, Bull. Math. Biol. 74 (4) (2012) 803–833, http://dx.doi.org/10.1007/s11538-011-9688-7.

[77] S. van der Stelt, A. Doelman, G. Hek, J.D.M. Rademacher, Rise and fall of periodic patterns for a generalized Klausmeier–Gray–Scott model, J. Nonlinear. Sci. 23 (1) (2013) 39–95, http://dx.doi.org/10.1007/s00332-012-9139-0.

[78] Y.R. Zelnik, S. Kinast, H. Yizhaq, G. Bel, E. Meron, Regime shifts in models of dryland vegetation, Philos. Trans. R. Soc. Lond. Ser. A Math. Phys. Eng. Sci. 371 (2004) (2013) 20120358, http://dx.doi.org/10.1098/rsta.2012.0358.

[79] I. Rodriguez-Iturbe, A. Porporato, L. Ridolfi, V. Isham, D.R. Coxi, Probabilistic modelling of water balance at a point: the role of climate, soil and vegetation, Proc. R. Soc. Lond. Ser. A Math. Phys. Eng. Sci. 455 (1990) (1999) 3789–3805, http://dx.doi.org/10.1098/rspa.1999.0477.

[80] G.D. Salvucci, Estimating the moisture dependence of root zone water loss using conditionally averaged precipitation, Water Resour. Res. 37 (5) (2001) 1357–1365, http://dx.doi.org/10.1029/2000WR900336.

[81] W. van Wijngaarden, Elephants, Trees, Grass, Grazers : Relationships Between Climate, Soils, Vegetation, and Large Herbivores in a Semi-Arid Savanna Ecosystem (Tsavo, Kenya) (Ph.D. thesis), International Institute for Aerospace Survey and Earth Sciences, Enschede, Netherlands, 1985.

[82] R. HilleRisLambers, M. Rietkerk, F. van den Bosch, H.H.T. Prins, H. de Kroon, Vegetation pattern formation in semi-arid grazing systems, Ecology 82 (1) (2001) 50–61, http://dx.doi.org/10.2307/2680085.

[83] M.J. Rossi, J.O. Ares, Water fluxes between inter-patches and vegetated mounds in flat semiarid landscapes, J. Hydrol. 546 (2017) 219–229, http://dx.doi.org/10.1016/j.jhydrol.2017.01.016.

[84] S. Thompson, G. Katul, A. Konings, L. Ridolfi, Unsteady overland flow on flat surfaces induced by spatial permeability contrasts, Adv. Water Resour. 34 (8) (2011) 1049–1058, http://dx.doi.org/10.1016/j.advwatres.2011.05.012.

[85] W.-J. Wang, W.-X. Huai, S. Thompson, G.G. Katul, Steady nonuniform shallow flow within emergent vegetation, Water Resour. Res. 51 (12) (2015) 10047–10064, http://dx.doi.org/10.1002/2015wr017658.

[86] E. Gilad, J. von Hardenberg, A. Provenzale, M. Shachak, E. Meron, A mathematical model of plants as ecosystem engineers, J. Theoret. Biol. 244 (4) (2007) 680–691, http://dx.doi.org/10.1016/j.jtbi.2006.08.006.

[87] J. Murray, Mathematical Biology, in: Biomathematics (Berlin), Springer-Verlag, 1989, http://dx.doi.org/10.2307/2348289.

[88] J.W. Cooley, P.A.W. Lewis, P.D. Welch, The fast Fourier transform and its applications, IEEE Trans. Educ. 12 (1) (1969) 27–34, http://dx.doi.org/10.1109/TE.1969.4320436.

[89] P. Chesson, R.L.E. Gebauer, S. Schwinning, N. Huntly, K. Wiegand, M.S.K. Ernest, A. Sher, A. Novoplansky, J.F. Weltzin, Resource pulses, species interactions, and diversity maintenance in arid and semi-arid environments, Oecologia 141 (2) (2004) 236–253, http://dx.doi.org/10.1007/s00442-004-1551-1.

[90] O. Lejeune, P. Couteron, R. Lefever, Short range co-operativity competing with long range inhibition explains vegetation patterns, Acta Oecol. 20 (3) (1999) 171–183, http://dx.doi.org/10.1016/S1146-609X(99)80030-7.

[91] W. Lewandrowski, T.E. Erickson, K.W. Dixon, J.C. Stevens, J. Firn, Increasing the germination envelope under water stress improves seedling emergence in two dominant grass species across different pulse rainfall events, J. Appl. Ecol. 54 (3) (2017) 997–1007, http://dx.doi.org/10.1111/1365-2664.12816.

[92] S. Ellner, A. Shmida, Why are adaptations for long-range seed dispersal rare in desert plants? Oecologia 51 (1) (1981) 133–144, http://dx.doi.org/10.1007/BF00344663.

[93] R.I. Maidment, D. Grimes, E. Black, E. Tarnavsky, M. Young, H. Greatrex, R.P. Allan, T. Stein, E. Nkonde, S. Senkunda, E.M.U. Alcántara, A new, long-term daily satellite-based rainfall dataset for operational monitoring in Africa, Sci. Data 4 (1) (2017) http://dx.doi.org/10.1038/sdata.2017.63.

[94] C. Dieulin, G. Mahé, J.-E. Paturel, S. Ejjiyar, Y. Tramblay, N. Rouché, B.E. Mansouri, A new 60-year 1940/1999 monthly-gridded rainfall data set for Africa, Water 11 (2) (2019) 387, http://dx.doi.org/10.3390/w11020387.

[95] E. Meron, Pattern-formation approach to modelling spatially extended ecosystems, Ecol. Model. 234 (2012) 70–82, http://dx.doi.org/10.1016/j.ecolmodel.2011.05.035, Modelling clonal plant growth: From Ecological concepts to Mathematics.

[96] E. Siero, A. Doelman, M.B. Eppinga, J.D.M. Rademacher, M. Rietkerk, K. Siteur, Striped pattern selection by advective reaction-diffusion systems: resilience of banded vegetation on slopes, Chaos 25 (3) (2015) 036411, http://dx.doi.org/10.1063/1.4914450.

[97] F. Borgogno, P. D'Odorico, F. Laio, L. Ridolfi, Mathematical models of vegetation pattern formation in ecohydrology, Rev. Geophys. 47 (2009) RG1005, http://dx.doi.org/10.1029/2007RG000256.

[98] R. Martinez-Garcia, C. Lopez, From scale-dependent feedbacks to long-range competition alone: a short review on pattern-forming mechanisms in arid ecosystems. arXiv:http://arxiv.org/abs/1801.01399v1.

[99] E. Gilad, M. Shachak, E. Meron, Dynamics and spatial organization of plant communities in water-limited systems, Theor. Popul. Biol. 72 (2) (2007) 214–230, http://dx.doi.org/10.1016/j.tpb.2007.05.002.

[100] E. Siero, Nonlocal grazing in patterned ecosystems, J. Theoret. Biol. 436 (2018) 64–71, http://dx.doi.org/10.1016/j.jtbi.2017.10.001.

[101] E. Siero, K. Siteur, A. Doelman, J. van de Koppel, M. Rietkerk, M.B. Eppinga, Grazing away the resilience of patterned ecosystems, Am. Nat. 193 (3) (2019) 472–480, http://dx.doi.org/10.1086/701669.